Check for updates

Batteries & Supercaps

Research Article
doi.org/10.1002/batt.202300336

Chemistry Europe
European Chemical Societies Publishing

www.batteries-supercaps.org

Special Collection

Reactive Interactions between the Ionic Liquid BMP-TFSI and a Na Surface

Katrin Forster-Tonigold,[a, b] Florian Buchner,[c] Axel Groß,[a, c] and R. Jürgen Behm*[c]

In order to obtain atomistic insights into the initial stages of the formation of the solid electrolyte interphase (SEI) in Na ion or Na metal batteries, we employ surface chemistry experiments and DFT calculations to study the interactions and reactions between a Na surface and the ionic liquid (IL) 1-butyl-1-methylpyrrolidinium bis(trifluoromethylsulfonyl)imide (BMP-TFSI), a candidate to be used as electrolyte in batteries. Oxygen-free Na thin films, which were grown on Ru(0001) and characterized by X-ray and ultraviolet photoelectron spectroscopy (XPS, UPS), can be understood as model of a Na-rich electrode. After deposition of submonolayer to multilayer BMP-TFSI films on the Na thin films at room temperature, XPS measurements revealed partial decomposition and the formation of a 'contact layer' at the Na surface, consisting of mainly TFSI-based decomposition products. By comparison to core level binding energies obtained from density functional theory calculations for energetically feasible reaction products, the constituents of the 'contact layer' were identified both as atomic fragments of TFSI (F, O, S) and as larger fragments of TFSI (NSO_2CF_3, $NSO_2CF_3SO_2$), presumably remaining at the surface due to kinetic barriers. Increasing the temperature results in cumulative decomposition towards the stable atomic species at or within the Na surface.

Introduction

Because of their very high energy density and long cycle life, lithium-ion batteries (LIBs) still dominate the market for energy storage systems. Nevertheless, as the resources of raw materials for LIBs are scarce, alternative battery systems are urgently needed. In recent years, tremendous progress has been made for sodium-ion batteries (SIBs).[1–6] In particular regarding cost, abundance and distribution of raw materials across the earth, SIBs possess distinct advantages over LIBs.[7] Besides, the chemical similarity of the two alkali metal ions Na^+ and Li^+ offers the possibility of a "drop-in" technology for SIBs, which can make use of similar working mechanisms and components in the battery application. Regarding the electrode materials typically hard carbon is used as anode and layered transition metal oxide, Prussian white/blue and analogues or vanadium phosphate are employed as cathode materials.[2–4,8,9]

Among the different electrolytes, which have been studied for SIBs, ionic liquids (ILs) (room temperature molten organic salts with a melting point below 100 °C)[10] are highly attractive candidates, due to their wide electrochemical stability, very low vapor pressure and good ionic conductivity.[11–15] For electrolytes consisting of sodium bis(trifluoromethanesulfonyl)imide (Na-TFSI) or sodium bis(fluorosulfonyl)imide (Na-FSI) dissolved either in 1-butyl-1-methylpyrrolidinium bis(trifluoromethanesulfonyl)imide (BMP-TFSI), in BMP-bis(fluorosulfonyl)imide (BMP-FSI) or in closely related ILs with slightly modified cations, promising results regarding the Na ion conductivity and the electrochemical performance have been obtained.[16–20] Insights into the Na ion conduction mechanism in an electrolyte consisting of Na-FSI dissolved in 1-methyl-1-propylpyrrolidinium – FSI have been obtained by a combined experimental and force field based molecular dynamics study.[21] Furthermore, density functional theory (DFT) calculations have been employed to elucidate the Na^+ transport mechanism of Na-TFSI in imidazolium based ILs.[22]

However, one of the remaining open questions in SIBs research concerns the complex reactive behavior at the electrode|electrolyte interface (EEI), which finally leads to the formation of the solid electrolyte interphase (SEI). The SEI is a decisive part for the functioning of the SIBs. Most earlier studies mainly concluded on the SEI quality from performance measurements with various electrolytes, and did not provide much molecular scale detail on the SEI components and formation mechanism.[23] IL-based electrolytes or electrolytes based on fluorinated molecules were reported to form a stable SEI on a Na-metal anode.[24,25] The composition of the SEI and variations therein for different formation conditions were studied in detail by different ex situ techniques, such as

[a] Dr. K. Forster-Tonigold, Prof. Dr. A. Groß
Helmholtz Institute Ulm Electrochemical Energy Storage (HIU)
Helmholtzstraße 11, 89081 Ulm (Germany)

[b] Dr. K. Forster-Tonigold
Karlsruhe Institute of Technology (KIT)
P.O. Box 3640, 76021 Karlsruhe (Germany)

[c] Dr. F. Buchner, Prof. Dr. A. Groß, Prof. Dr. R. J. Behm
Institute of Theoretical Chemistry
Ulm University
Oberberghof 7, 89081 Ulm (Germany)
E-mail: juergen.behm@uni-ulm.de

Supporting information for this article is available on the WWW under https://doi.org/10.1002/batt.202300336

Special Collection This publication is part of a joint Special Collection of ChemSusChem, Batteries& Supercaps, and Energy Technology including invited contributions focusing on the "International Conference on Sodium Batteries (ICNaB)"

© 2023 The Authors. Batteries & Supercaps published by Wiley-VCH GmbH. This is an open access article under the terms of the Creative Commons Attribution Non-Commercial NoDerivs License, which permits use and distribution in any medium, provided the original work is properly cited, the use is non-commercial and no modifications or adaptations are made.

© 2023 The Authors. Batteries & Supercaps published by Wiley-VCH GmbH

vibrational or photoelectron spectroscopy, microscopy techniques and also by molecular dynamics simulations. Employing X-ray diffraction (XRD) and photoelectron spectroscopy (XPS) to identify NaF as reaction product, Hosokawa et al. investigated the reactivity of Na towards a TFSI-based IL upon immersing metallic Na into the IL.[26] In a comparable approach, Forsyth et al. identified SEI components formed on a Na metal anode after cycling in other electrolytes with various imide based Na-salt additives by XPS and infrared spectroscopy.[27] Besides NaF and Na_2O compounds, they also found inorganic oxo-species and remaining C–F species within the SEI of the electrolyte with a Na-TFSI additive. Furthermore, water additives were found to have an impact on the SEI composition in IL based electrolytes.[28] Although such post-mortem studies of the SEI composition can provide valuable insights into the composition of the SEI, they are less useful for the identification of the SEI formation process, in particular when focusing on the initial stages.

On the other hand, detailed in situ studies of the SEI formation, revealing the underlying mechanisms on an atomic level are hardly possible for the real environment of the battery. Thus, to obtain molecular scale insights into the processes occurring at the interface and the intermediates formed during these processes, the complexity of the system needs to be reduced. Therefore, we made use of well-defined model systems to study the surface chemistry at the EEI under ultrahigh vacuum (UHV) conditions, employing surface science techniques such as scanning tunneling microscopy (STM) or photoelectron spectroscopy (XPS, UPS) and using structurally and chemically well-defined, atomically smooth single crystal surfaces. We combined this experimental study with corresponding density functional theory (DFT) calculations.[29–33]

In the present study, we investigate the interaction between bulk-like Na films and the IL BMP-TFSI[18] as representative for a Na metal or a Na-rich electrode with an ultrathin Na layer on top and a battery-relevant electrolyte. First, we will present XPS and UPS results characterizing the Na films deposited on Ru(0001), which underline the close similarity between these films and a Na bulk surface (Section Preparation of well-defined, bulk-like Na films). We then characterize the adsorption and interaction of BMP-TFSI mono-/multilayer films on/with a pre-deposited Na film by XPS (Section Interaction of a multilayer BMP-TFSI film with a Na film surface), aiming at the identification of possible decomposition products. This is followed by annealing experiments that provide further information on possible decomposition products and their formation (Section Interaction of ultrathin BMP-TFSI films with a Na surface and thermal activation). Next, we present results of DFT calculations of the adsorption configuration and energy of BMP-TFSI ion pairs in interaction with a Na surface (Section Intact BMP-TFSI on Na(0001)) and of different possible decomposition products of BMP-TFSI on this surface (Section Possible decomposition reactions of BMP-TFSI on Na(0001)). Subsequently, we compute core level binding energies of probable reaction products (Section Calculated core level binding energies) and compare these with the experimental findings in the XPS experiments (Section Comparison of experimental and calculated core level binding energies of decomposition products) to unambiguously identify the products and long-living intermediates resulting from this reaction. Here, we also comment on the applicability and relevance of these findings for real battery systems. Finally, the results are shortly summarized and final conclusions are drawn (Section Conclusion). Experimental and computational details are summarized in the Methods Section at the end.

Overall, this work provides a detailed atomic/molecular scale picture of the reactive interaction of an IL film with a Na model anode, which is considered as the initial stage of the SEI formation at the electrode | electrolyte interface.

Results

Experimental results

Preparation of well-defined, bulk-like Na films

As a first step we checked whether Na deposition on a single crystalline Ru(0001) surface at room temperature (r.t.) leads to clean Na thin films, employing X-ray and ultraviolet photoelectron spectroscopy (XPS and UPS) (Figure 1). For testing the evaporator source we first prepared very thin Na films (thicknesses $d \leq 4$ Å), before generating thicker, bulk-like films with thicknesses up to ~27 Å. For the latter films we moved the evaporator closer to the sample. Considering the thickness of the final film, one can safely assume that the underlying Ru surface is completely covered by Na. This is highly important for the objective of the present study, which aims at the characterization of the interaction between BMP-TFSI and Na (see next section), to exclude any effects of the Ru(0001) substrate.

To begin with, we analyzed the purity of the Na films by XPS (Figure 1a) during stepwise deposition of small amounts of Na ($d \leq 4$ Å, solid lines with different grey shades). The thickness of the Na films was derived from the damping of the Ru 3d electron intensities as described in the experimental section, assuming a homogeneous film growth. For the initial Na deposition steps, the Na 1s spectra show a single peak (Figure 1a, left upper panel), which gradually increases in intensity with increasing deposition. The peak is first centered at a binding energy (BE) of around 1072.3 eV, and then shifts towards lower BEs of around 1072.0 eV, which is characteristic for the evolution of metallic Na.[34–39] When generating thicker Na films (10, 15 and 27 Å (blue solid line)), pronounced features appear at the high energy side of the main peak, which have been assigned to the additional excitation of bulk plasmons ($\hbar\omega_{P,bulk}$ and $-2\hbar\omega_{bulk}$) and of surface plasmons ($\hbar\omega_{surf}$ and $-2\hbar\omega_{surf}$).[34–38] These features and their relative intensities have been considered as clear evidence for a metallic character of the thicker Na films. For information on the Na film thickness we included the Ru 3d spectra before and after the last Na deposition step (see inset in Figure 1a), which reveal a damping by about 45%, equivalent with a Na film thickness of ~27 Å. The corresponding Na 2s and Na 2p spectra for this Na film (blue solid lines in Figure 1b) show peaks due to metallic Na at BEs of 63.6 and 30.8 eV (cf. refs. [37, 38]), respectively, together

© 2023 The Authors. Batteries & Supercaps published by Wiley-VCH GmbH

25666223, 2023, 12, Downloaded from https://chemistry-europe.onlinelibrary.wiley.com/doi/10.1002/batt.202300336 by Cochrane Germany, Wiley Online Library on [06/12/2023]. See the Terms and Conditions (https://onlinelibrary.wiley.com/terms-and-conditions) on Wiley Online Library for rules of use; OA articles are governed by the applicable Creative Commons License

Research Article
doi.org/10.1002/batt.202300336
Chemistry Europe
European Chemical Societies Publishing

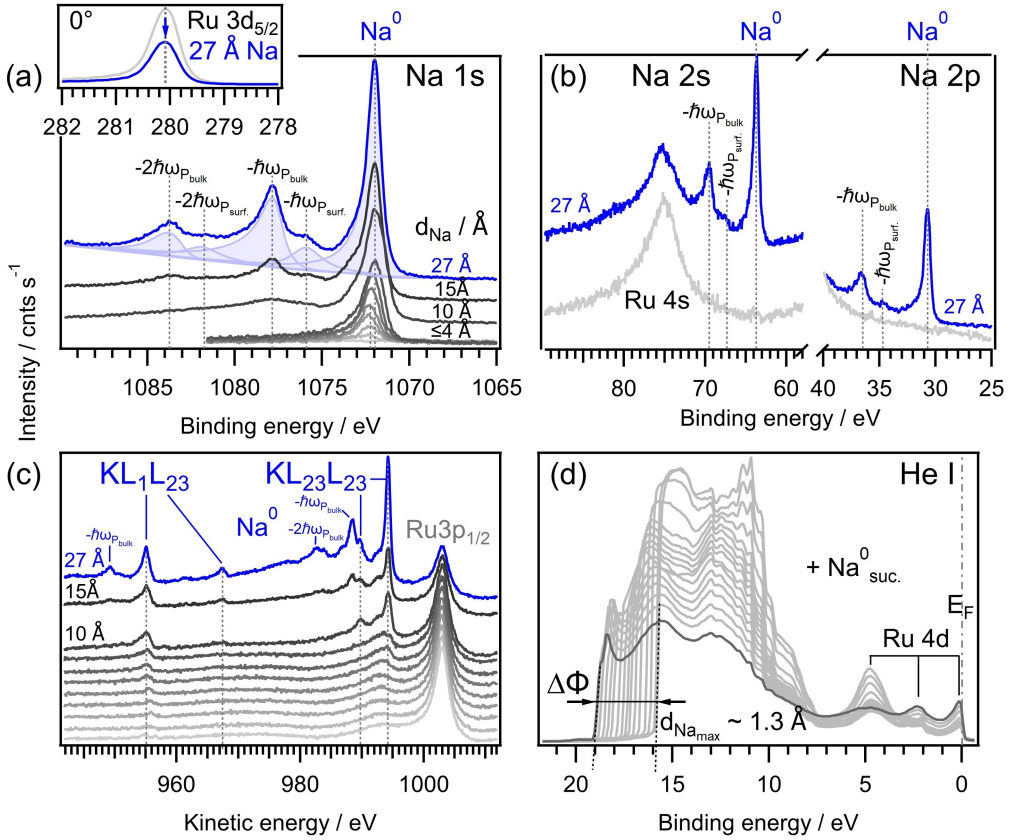

Figure 1. UPS and XPS spectra of Na films of different thicknesses obtained by Na vapor deposition on a Ru(0001) substrate at r.t. (He I line and monochromatized Al–K_a radiation, emission 70° with respect to the surface normal, increasing thickness from grey to black).

with the corresponding bulk and surface plasmon loss features ($-\hbar\omega_{bulk}$ and $-\hbar\omega_{surf}$).[38] In addition, during stepwise Na deposition, KLL Auger transitions appear at kinetic energies of around 994 and 990 eV ($KL_{23}L_{23}$) and at 967 and 955 eV (KL_1L_{23}), respectively (Figure 1c, film thicknesses as in Figure 1a). The additional features in these spectra are again due to the different plasmon losses ($-\hbar\omega_{bulk}$ and $-\hbar\omega_{surf}$) described above, further supporting the metallic character of these Na films. For non-metallic compounds such as Na_2O, a rather large chemical shift of around 4.5 eV would be expected with dominant Auger transitions at kinetic energies of 990.0 and 950.8 eV,[37] respectively, which were not obtained in the present spectra. Hence, we can exclude larger amounts of oxide contaminations.

Finally, we recorded valence band (UPS) spectra of ultrathin Na films (Figure 1d) with thicknesses $\leq$1.3 Å, using He I radiation (21.21 eV) (Figure 1d). The spectrum of the pristine Ru(0001) substrate (black solid line) displays peaks at ~0.3, 2.6, and 5.0 eV (Ru 4d band), in agreement with literature.[40–42] The work function Φ was determined from the cut-off energy ($E_{cut\text{-}off}$) of 16.0 eV to 5.2 $\pm$ 0.1 eV ($\Phi_{Ru(0001)} = h\nu - E_{cut\text{-}off}$). As expected, during stepwise vapor deposition of sub-monolayer amounts of Na the work function Φ gradually decreases (grey solid lines). After the last deposition step (d_{Na} ~ 1.3 Å, dark grey solid line) the work function Φ had decreased by about 3 eV to Φ_{Na} = 2.2 eV, which is in good agreement with the value given by Garfunkel et al. for Na coverages $\geq$ 0.5 monolayer (ML) on Ag(110).[43]

Overall, clean, oxygen-free Na thin films with thicknesses up to around 27 Å were prepared on a Ru(0001) single crystalline surface and carefully characterized by XPS and UPS measurements. These bulk-like Na films, which completely cover the Ru surface, are considered as well-suited Na metal model systems for Na anodes in post-Li batteries. In the following, we will explore the interaction of a model electrolyte (BMP-TFSI) with these Na model systems.

Interaction of a multilayer BMP-TFSI film with a Na film surface

In a first control experiment we deposited a thick multi-layer BMP-TFSI film (thickness about 8 ML) on the freshly prepared Na film substrate (Na thickness ca. 8 Å) at 80 K. XP spectra recorded from this film are presented in Figure 2. In addition, the figure displays a molecular representation of BMP-TFSI on top of the panel. To enhance the visibility of the adsorbate signals with respect to the Ru $3d_{3/2}$ substrate signal, the C 1s spectra were recorded in grazing emission (electron emission angle θ = 70° with respect to the surface normal, information depth ID = 3×mean free path $\lambda \times \cos\theta$, Figure 2, left panel), while the F 1s, O 1s, N 1s and S 2p core level spectra were acquired at normal emission (0° with respect to the surface normal), where

© 2023 The Authors. Batteries & Supercaps published by Wiley-VCH GmbH

25666223, 2023, 12, Downloaded from https://chemistry-europe.onlinelibrary.wiley.com/doi/10.1002/batt.202300336 by Cochrane Germany, Wiley Online Library on [06/12/2023]. See the Terms and Conditions (https://onlinelibrary.wiley.com/terms-and-conditions) on Wiley Online Library for rules of use; OA articles are governed by the applicable Creative Commons License

Research Article
doi.org/10.1002/batt.202300336
Chemistry Europe
European Chemical Societies Publishing

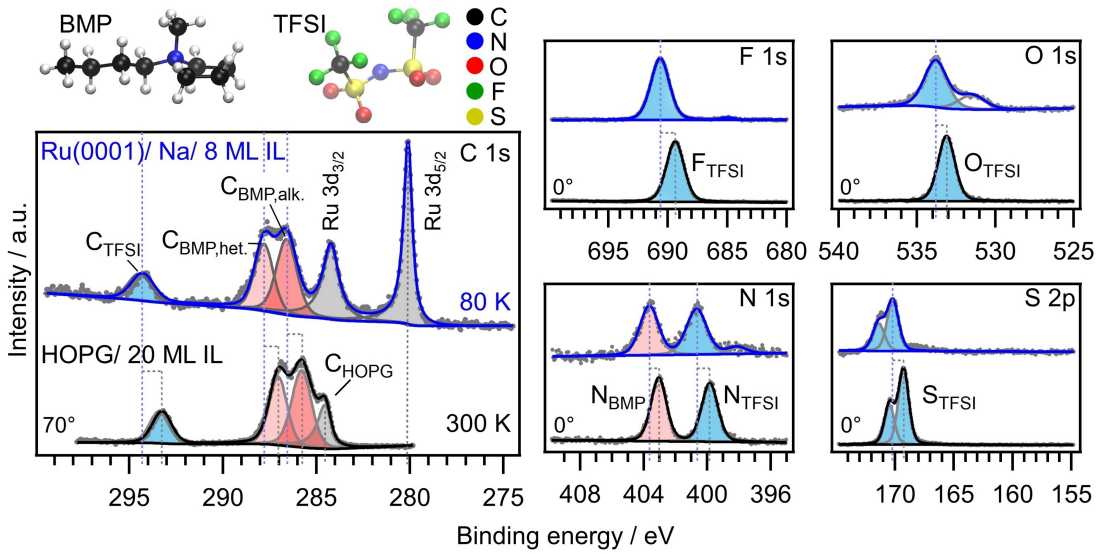

Figure 2. XP spectra of a BMP-TFSI multilayer film (thickness and deposition temperature are indicated in the panels) on HOPG and on a Na film (Na film thickness 8 Å).

the absolute intensities are higher (Figure 2, right panels). The BEs of all BMP-TFSI related peaks are listed in Table 1, using typical abbreviations for their origin such as F_{TFSI}, O_{TFSI}, N_{TFSI}, N_{BMP}, C_{TFSI}, $C_{BMP,alk}$, $C_{BMP,het}$ and S_{TFSI} for the atoms of the anion and the cation, respectively. IL-related XPS peaks of adsorbed BMP-TFSI multilayers had also been reported in previous publications, where the nature of the different peaks was explained in detail as well.[29,31,32,44] For comparison, we also show similar type spectra recorded on a BMP-TFSI multilayer film adsorbed on graphite(0001) (HOPG) in the lower panels of Figure 2.

We start with the C 1s spectra, which comprise information on both the BMP cation and the TFSI anion. Beside the strongly damped Ru 3d doublet (Ru $3d_{5/2}$: 280.1 eV, Ru $3d_{3/2}$: 284.3 eV[34]), they reveal two peaks related to the 5 alkyl-like C-atoms ($C_{BMP,alk}$,filled red) on the one hand and to the 4 C-atoms neighbored to the N-atom of the BMP cation ($C_{BMP,het}$, filled light red) on the other hand. In addition, there is a smaller peak at the high BE side, which is due to the C-atoms in the CF_3 groups of the anion ($C_{TFSI,}$ filled cyan). Both the significantly higher binding energy (BE) of this peak and the much lower intensity correspond to expectations, considering the high electronegativity of the F atoms in the CF_3 groups and the fact that only 2 C atoms per molecule ion pair contribute to this signal. The agreement of the integrated peak intensities of C_{TFSI}, $C_{BMP,het}$ and $C_{BMP,alkyl}$ of about 2:4:5 with the stoichiometric ratio of the corresponding atoms in the ionic liquid provides strong evidence that the spectrum is dominated by molecularly adsorbed BMP-TFSI species.

The spectrum of the C 1s region recorded on a BMP-TFSI multilayer film deposited on HOPG (Figure 2, black solid line, film thickness about 20 ML) shows the substrate peak at 284.6 eV,[34] which is almost completely damped, in contrast to the Ru 3d and Na 1s peaks for the BMP-TFSI covered on the Na surface (Figure S7, Supporting Information, BMP-TFSI film thickness about 8 ML). The spectrum contains the same three IL-related peaks discussed above, with the same intensity ratios, supporting our above conclusion of a molecularly intact adsorption (see Refs. [29, 31]). Interestingly, the IL-related peaks of the BMP-TFSI multilayer on Na are slightly up-shifted

Table 1. Binding energies of the different XPS peaks of a molecularly adsorbed BMP-TFSI multilayer film on HOPG and on a Na-film covered Ru(0001) substrate, respectively, prepared by deposition at 80 K. The abbreviations given in the right column will be used throughout the paper to refer to the respective peaks.

Core level	BE_{HOPG} [eV]	BE_{Na} [eV]	Configuration	Notation
C 1s	285.8	286.6	–C–C–	$C_{BMP,alk}$
C 1s	287.1	287.8	–C–N–	$C_{BMP,het}$
N 1s	403.1	403.7	–C–N–	N_{BMP}
C 1s	293.4	294.3	$–CF_3$	C_{TFSI}
N 1s	399.9	400.7	–S–N–S–	N_{TFSI}
F 1s	689.4	690.6	$–CF_3$	F_{TFSI}
O 1s	533.2	533.8	$–SO_2–$	O_{TFSI}
S $2p_{3/2}$	169.3	170.2	$–SO_2–$	S_{TFSI}

© 2023 The Authors. Batteries & Supercaps published by Wiley-VCH GmbH

25666223, 2023, 12, Downloaded from https://chemistry-europe.onlinelibrary.wiley.com/doi/10.1002/batt.202300336 by Cochrane Germany, Wiley Online Library on [06/12/2023]. See the Terms and Conditions (https://onlinelibrary.wiley.com/terms-and-conditions) on Wiley Online Library for rules of use; OA articles are governed by the applicable Creative Commons License

compared to the same film on HOPG. Reasons for this up-shift will be discussed later.

Similar spectra were recorded also in the F 1s, O 1s, N 1s and S 2p regions (see Figure 2, right panels). These spectra reveal the typical F_{TFSI}, O_{TFSI}, N_{TFSI}, N_{BMP} and S_{TFSI} peaks as observed previously for BMP-TFSI multilayer films on other substrates such as Ag(111), HOPG and Mg,[29,31,32,44] and also the intensity ratios fit almost perfectly to the stoichiometric ratios, supporting our above claim of molecularly intact adsorption of BMP-TFSI under these conditions. Also for these spectra, the respective BEs are compiled in Table 1.

Furthermore, comparison with similar spectra recorded on a multilayer BMP-TFSI film on HOPG (black spectra) reveals slight up-shifts of the peaks as compared to BMP-TFSI on HOPG, which are illustrated by the shifts in the vertical lines. Such up-shifts compared to the BEs of BMP-TFSI multilayer films on HOPG had already been observed upon interaction of BMP-TFSI with a Mg-film covered Ru surface,[32] where this phenomenon was explained by vacuum level pinning, i.e., by a pinning of the electronic states of the weakly bound adsorbate species to the vacuum level of the solid substrate. In the case of a substrate with lower work function, as it is the case for Na/Ru(0001) compared to HOPG, alignment of the vacuum levels leads to an up-shift of the Fermi level E_F of the solid as compared to a substrate with higher work function. Considering that the binding energy is calculated with respect to E_F, an up-shift of E_F results in a higher BE of the adsorbate-related core levels. On the other hand, such up-shifts should be identical for all peaks, while experimentally we find differences in the range of a few tenths of an eV. Therefore, vacuum level pinning cannot be the only contribution for the observed shifts. Further possibilities for the physical origin of these differences will be discussed in more detail in a forthcoming publication.

Overall, the XPS measurements of bulk-like BMP-TFSI multilayers adsorbed on a Na film covered Ru(0001) substrate reveal molecularly intact adsorbed BMP-TFSI species. Compared to BMP-TFSI multilayers on other substrates such as HOPG they differ by a slight shift in the BEs of the IL-related core levels, which are assigned to a combination of vacuum level pinning effects and individual shifts.

Interaction of ultrathin BMP-TFSI films with a Na surface and thermal activation

To study the chemical reactions and interactions between BMP-TFSI and Na directly at the interface, we stepwise deposited an ultrathin BMP-TFSI film with a final thickness of 1.7 ML at r.t., with 0.3 ML in a first step and 1.4 ML in a second step. Different from the situation in Figure 2, deposition was performed with the sample at r.t. XP spectra recorded for these films after deposition and after subsequent stepwise annealing to 420 K, 470 K and 570 K are shown in Figure 3. The TFSI-related peaks in Figure 3 are filled cyan, the BMP-related peaks red, possible larger fragments with yellow-blue gradient and smaller fragments such as binary salts yellow.

In the Na 1s regime the XP spectrum recorded for the pure Na film shows peaks characteristic for metallic Na as described in detail in the previous section. After deposition of 0.3 ML BMP-TFSI on this Na film the peak at 1072.0 eV, which is attributed to the Na 1s core level of metallic Na (see above), loses about 40% of its intensity and a new peak appears at around 1073.0 eV. Based on reports of Na 1s BEs of 1072.5 or 1072.9 eV for Na_2O or Na_2O_2,[37,45] this can be assigned to Na^+ species. The intensity of this peak further increases after the second deposition step and even more after subsequent heating to 420 K and 470 K, on the expense of the low-BE peak, as expected for an increasing formation of ionic Na species.

We would like to note that not only the intensity of the peak attributed to Na^+, but also the total intensity of the Na 1s peaks increases during heating, and thus during partial decomposition of the BMP-TFSI film. This was not expected and cannot be explained by experimental effects such as slight variations in the position/orientation of the sample with respect to the spectrometer. A comparable intensity increase of the Na 1s peak was reported also during increasing O_2 exposure to a Na film by Hwang et al.,[45] but without providing an explanation on the underlying physical effects. Therefore, we will refrain from a quantitative discussion of the measured intensities and focus on trends.

In the F 1s region we find two peaks after the initial deposition of 0.3 ML BMP-TFSI. The first peak at 690.9 eV can be attributed to the F atoms of intact TFSI, as the BE is comparable to that of F 1s in a BMP-TFSI multilayer deposited on Na at 80 K (F_{TFSI}: 690.6 eV, see Table 1 in the previous section). Furthermore, this peak may contain also contributions from initial decomposition products of TFSI in which the F atoms are in a similar chemical environment as in the parent structure. A second peak with comparable intensity appears at 685.8 eV. This peak must be due to decomposition products of TFSI ($F_{TFSI,dec-1}$) with a very different chemical environment of the F atoms, as evident from the significant shift. Most likely, this results from a compound with a chemical environment close to that of NaF, as the F 1s BE of NaF is reported to be 684.5 eV.[34,46,47] Except for a slight up-shift of the $F_{TFSI,dec-1}$ peak, both the positions and the intensity ratio (around 1:1) of the two peaks essentially persist, if additional 1.4 ML of BMP-TFSI are deposited. Upon heating, both peaks shift to slightly lower BEs again, by −0.6 eV and −0.3 eV for F_{TFSI} and $F_{TFSI,dec-1}$, respectively. Furthermore, the F_{TFSI} peak intensity declines considerably upon heating and is essentially gone after heating to 470 K, whereas the intensity of the $F_{TFSI,dec-1}$ peak increases. Hence, at this point the decomposition of adsorbed TFSI into fragments with a significantly different chemical environment of the F atoms is essentially completed. Upon further heating to 570 K also this peak loses intensity, indicative of the desorption of F-containing fragments in this temperature range.

In the S 2p regime, which contains the S $2p_{1/2}$ and the S $2p_{3/2}$ peaks ($\Delta BE = \sim 1.25$ eV), we will focus on the S $2p_{3/2}$ peaks. Here, we find three different low-intensity peaks emerging at about 162.0 eV, 166.0 eV and 170.0 eV after deposition of 0.3 ML BMP-TFSI. After deposition of in total 1.7 ML BMP-TFSI the peaks are more pronounced, with the peak at the low BE

© 2023 The Authors. Batteries & Supercaps published by Wiley-VCH GmbH

25666223, 2023, 12, Downloaded from https://chemistry-europe.onlinelibrary.wiley.com/doi/10.1002/batt.202300336 by Cochrane Germany, Wiley Online Library on [06/12/2023]. See the Terms and Conditions (https://onlinelibrary.wiley.com/terms-and-conditions) on Wiley Online Library for rules of use; OA articles are governed by the applicable Creative Commons License

Research Article
doi.org/10.1002/batt.202300336

Chemistry Europe
European Chemical Societies Publishing

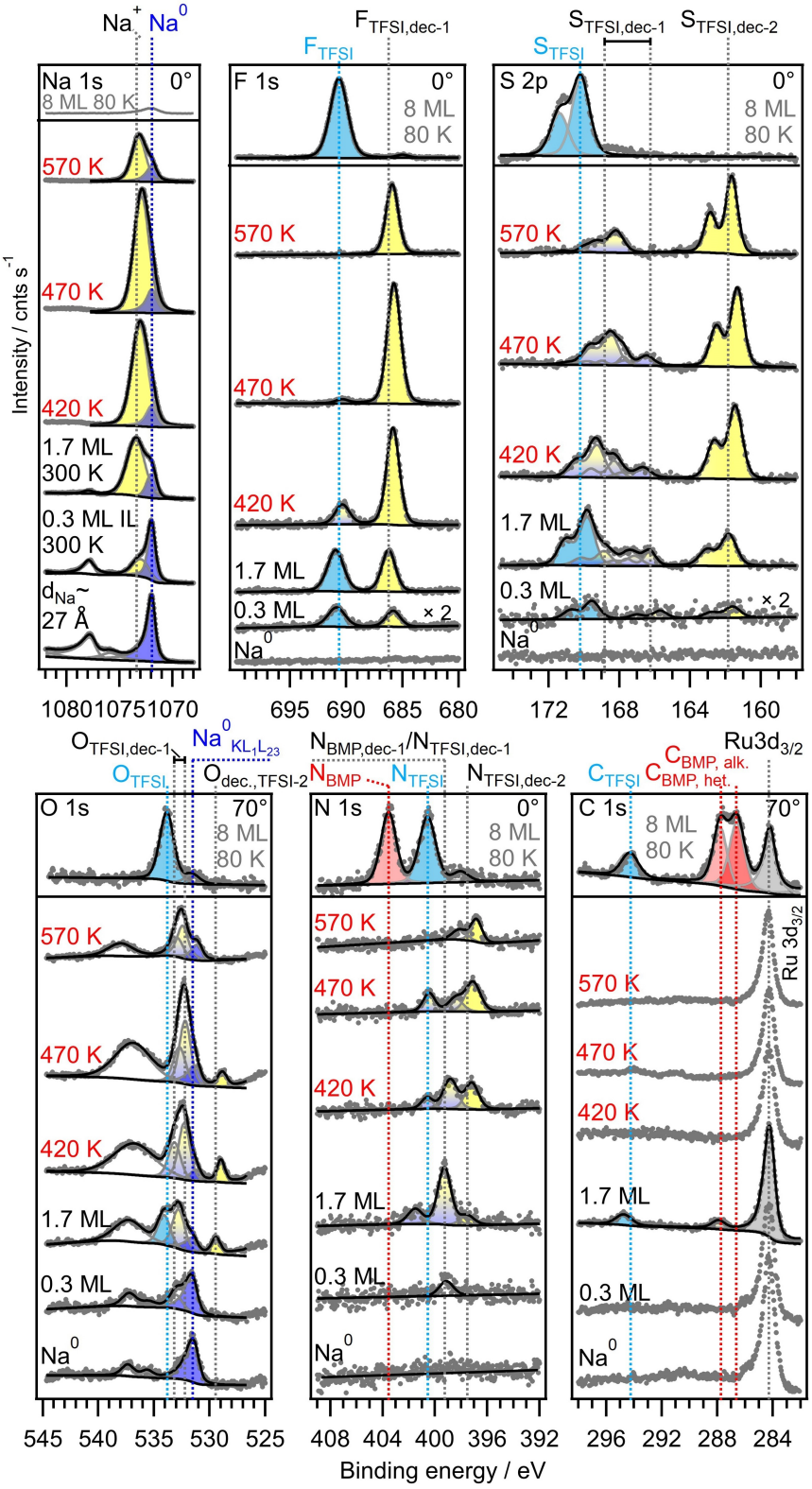

Figure 3. Na 1s, F 1s, S 2p, O 1s, N 1s and C 1s core level spectra of an adsorbed ultrathin BMP-TFSI film on a Na film (Na film thickness about 27 Å) after stepwise deposition of 0.3 ML and 1.7 ML BMP-TFSI in total at r.t. and upon successive annealing to 420 K, 470 K and 570 K. For comparison, the respective core level spectra of a thick adsorbed multilayer BMP-TFSI film (8 ML) deposited on a Na film at 80 K (Figure 2) are shown at the top of each panel. The red and blue dotted lines indicate the BEs of the respective peaks in a multilayer BMP-TFSI film after deposition at 80 K (Figure 2). Grey dotted lines refer to decomposition products that are explained in the text. If existent at that point, they are adjusted to the BE of the peak after deposition of 1.7 ML (colors: TFSI-related peaks filled cyan, BMP-related peaks filled red, possible larger fragments filled with yellow-blue gradient, smaller fragments filled yellow).

© 2023 The Authors. Batteries & Supercaps published by Wiley-VCH GmbH

25666223, 2023, 12, Downloaded from https://chemistry-europe.onlinelibrary.wiley.com/doi/10.1002/batt.202300336 by Cochrane Germany, Wiley Online Library on [06/12/2023]. See the Terms and Conditions (https://onlinelibrary.wiley.com/terms-and-conditions) on Wiley Online Library for rules of use; OA articles are governed by the applicable Creative Commons License

side appearing at 161.8 eV, that at the high BE side at 169.8 eV. The latter peak occurs at a BE which is slightly lower than the S 2p BE of intact BMP-TFSI multilayers adsorbed at 80 K ($S_{TFSI,}$ 170.2 eV, see Table 1). Therefore, we attribute it to intact TFSI that is directly bound to the Na surface or in the second layer. Alternatively, it may be related to initial decomposition products of TFSI in which the chemical environment of at least one of the two TFSI-related S atoms is still comparable to that within intact TFSI. The peak at 161.8 eV ($S_{TFSI,dec-2}$) is assigned to reduced S containing species, most probably to Na_2S, whose S $2p_{3/2}$ BE was reported to 161.8 eV[48] or 160.6 eV.[49]

Furthermore, deconvolution of the spectrum yields three peaks in the range between around 165 and 171 eV, (166.3, 167.2 and 168.9 eV, see below), in addition to the peak at 169.8 eV. The interval is marked on top of the panel. These peaks, referred to as $S_{TFSI,dec-1}$, and that at 161.8 eV ($S_{TFSI,dec-2}$) must be due to decomposition products of TFSI with different chemical environment of the S atoms. The BE of the peak at 166.3 eV matches the S $2p_{3/2}$ BE of sulfur dioxide adsorbed on Ni(111),[50] it is also very close to that of sodium sulfite which was reported at 166.5 eV[48] or 166.6 eV.[51] Therefore, we relate the peak at 166.3 eV to decomposition products of TFSI that contain $-SO_x$ groups. Furthermore, peak fitting of the 1.7 ML spectrum requires two additional peaks to match the experimental spectrum in the range of 165–168 eV. The best fit was obtained for BEs of around 168.9 eV and 167.2 eV, respectively, where the BEs may vary somewhat. This range is typical for sulfates or sulfites.[51,52] Upon annealing to 420 K, 470 K or 570 K, the peaks in the higher BE region (S_{TFSI} and $S_{TFSI,dec-1}$) decline, while an increase in intensity is observed for the $S_{TFSI,dec-2}$ peak, reflecting the progressive decomposition of TFSI via different intermediate species, summarized here under TFSI,dec-1, to thermally more stable adsorbed TFSI,dec-2 products.

In the O 1s region we identified four different peaks after deposition of BMP-TFSI, where one of them (531.6 eV) is assigned to the Na^0-KL_1L_{23} Auger line of metallic Na surface,[37] and the other three are attributed to different oxygen states. In addition, there are two plasmon loss features at around 535.6 eV and 537.3 eV related to the Auger line. Starting with the Na-related signals the Auger line of metallic Na gets considerably smaller if 0.3 and finally 1.7 ML BMP-TFSI are deposited and remains at about this level if the IL covered surface is heated to 420 K, 470 K and 570 K, respectively. Apparently, small amounts of metallic Na^0 are still present under these conditions. This interpretation is supported also by the gradual decrease of the plasmon loss features upon deposition of BMP-TFSI, which is clearly visible in Figure 1(a) and also for the Na 1s line at 1072.0 eV. In contrast, the loss features related to the Na-KL_1L_{23} Auger line, which are clearly visible for the bare Na film (Figure 3), are covered by a broad peak emerging at about 537.0 eV upon deposition of BMP-TFSI, and cannot be resolved any more. This broad feature might be attributed to the Na^+-KL_1L_{23} Auger line of Na^+-containing decomposition products. As pointed out in Ref. [37], the kinetic energy of such Auger processes is down-shifted by about 4.5 eV for Na_2O and by about 6 eV for NaOH with respect to its value for metallic Na, resulting in a similar up-shift in the BE scale.

Moving on to the O-related peaks, after deposition of 1.7 ML BMP-TFSI we find three peaks at 529.4 eV ($O_{TFSI,dec-2}$), at 532.8 eV ($O_{TFSI,dec-1}$), and at 534.1 eV (O_{TFSI}) (Figure 3). The first peak, which appears after deposition of in total 1.7 ML BMP-TFSI, is most probably due to $Na^{\delta+}$–$O^{\delta-}$ compounds, as the O 1s BE for Na_2O is reported to be in a similar energy range, at around 528.8[45] or 529.7 eV.[37] The second peak at 532.8 eV, which appears already after deposition of 0.3 ML BMP-TFSI, must be due to a decomposition product of TFSI as well, where the difference in the chemical environment is less pronounced than in the $Na^{\delta+}$–$O^{\delta-}$ compound. Therefore, we expect this to be an earlier decomposition product. Considering its width, this peak seems to consist of two closely neighbored peaks, indicative of two species with slightly different neighborhoods.f Finally, the peak at 534.1 eV, which is also clearly visible only after the second deposition step to 1.7 ML BMP-TFSI, is attributed to intact TFSI or to initial decomposition products with a chemical environment of the O atoms very close to that of TFSI, as the BE of 534.1 eV is rather close to the O 1s BE in TFSI in a multilayer adsorbed on Na(0001) at 80 K (533.8 eV, see Table 1). After heating to 420 K and 470 K, both the $O_{TFSI,dec-1}$ peak with its two components and the low-BE $O_{TFSI,dec-2}$ peak persist, but according to peak fitting show a slight down-shift in their respective BEs to 532.3 and 529.0 eV. On the other hand, the O_{TFSI} peak essentially disappeared already after the first heating step, indicative of complete decomposition of adsorbed TFSI at this point. At this point, an additional peak at 533.2 eV is needed for a proper fit of the broad spectral feature between 531 and 534 eV, indicative for the formation of another TFSI decomposition product. We refer to this product as $O_{TFSI,dec-1}$ as well, since together with the peak at 532.3 eV it results in the broad spectral feature mentioned above, although it must be different in the exact chemical nature. The respective energy interval is marked on top of the panel. Finally, the total O 1s intensity decreased considerably upon heating to 570 K, which must be due to considerable desorption of O-containing or O- and F-containing fragments in this temperature range.

In the N 1s regime we only find a single small peak at around 399.1 eV after deposition of 0.3 ML BMP-TFSI, which increases significantly in intensity after the next deposition step of additional 1.4 ML BMP-TFSI and slightly shifts to 399.3 eV. Based on the BE, it must be due to decomposition products of either BMP or TFSI, since the N 1s BE of adsorbed BMP and adsorbed TFSI are around 403.7 eV and 400.7 eV (BMP-TFSI multilayer, see Table 1), respectively. As shown in a previous study,[33] decomposition products of BMP and of Li-bonded decomposition products of TFSI can have N 1s BEs that are in this range. We expect that the same can be true also for Na bonded TFSI decomposition products. Interestingly, there is no peak at a BE characteristic for molecularly adsorbed BMP, which would be expected at around 403.7 eV (see Table 1), indicating that BMP instantaneously decomposes at r.t. in contact with the Na surface. From mass balance reasons this also means that the peak at around 399 eV contains significant contributions from an adsorbed decomposition product of BMP.[33] Furthermore, for this film two small peaks can be identified at around 397.6 eV and 401.5 eV, respectively. The high energy peak at

© 2023 The Authors. Batteries & Supercaps published by Wiley-VCH GmbH

25666223, 2023, 12, Downloaded from https://chemistry-europe.onlinelibrary.wiley.com/doi/10.1002/batt.202300336 by Cochrane Germany, Wiley Online Library on [06/12/2023]. See the Terms and Conditions (https://onlinelibrary.wiley.com/terms-and-conditions) on Wiley Online Library for rules of use; OA articles are governed by the applicable Creative Commons License

401.5 eV (N_{TFSI}) can be assigned to intact TFSI in contact with or close to the Na surface, as its N 1s BE is close to the BE of intact TFSI in a BMP-TFSI multilayer deposited at 80 K (400.7 eV, see Table 1). Upon heating, the intensity of the peak at 397.6 eV increases, whereas the intensity of the peak at 399.3 eV decreases, which might indicate a gradual transformation from an intermediate decomposition product to a thermodynamically (more) stable product that persists even upon heating to 570 K. We attribute the low BE peak at ~397.6 eV to decomposition products of TFSI based on the findings of our previous study where we identified a reaction intermediate with a C–N bond with a comparable N 1s BE[33] (see also our calculations summarized in the section Calculated core level binding energies). This also means that the BMP based decomposition products were mostly desorbed at 570 K. A comparable mechanism was revealed for the Li-induced decomposition of TFSI within a BMP-TFSI multilayer.[33] After heating to 570 K also the N_{TFSI} peak is gone, as expected from the BMP-TFSI evaporation temperature 470 K.

Finally, the C 1s region is almost featureless after Na deposition and after deposition of 0.3 ML BMP-TFSI, apart from the peak at 284.3 eV, which is assigned to the Ru 3d electron, but which may contain also contributions from ubiquitous carbon. After deposition of in total 1.7 ML BMP-TFSI, two additional peaks at around 287.9 eV and 294.7 eV emerge with rather low relative intensities. The peak at high BE (C_{TFSI}) can be related to intact TFSI or to fragments which largely maintain the chemical environment of the carbon atoms in that moiety, as the BE only differs by a few tenths of an eV from the respective value of TFSI in the BMP-TFSI multilayer on the Na film (294.3 eV after deposition at 80 K, see Table 1). The second peak at around 288 eV is assigned to C atoms in C–N bonds, as they were observed for intact BMP (287.8 eV for $C_{BMP,het.}$ in the BMP-TFSI multilayer on a Na film). Interestingly, there is no peak at the position of $C_{BMP,alk}$ signal (286.6 eV in the BMP-TFSI multilayer on a Na film), indicating that the BMP ring is no longer intact and that a significant part of these carbon species have desorbed. After heating to 420 K the new peaks are no longer visible, indicating the complete decomposition of BMP-TFSI and the desorption of most of the C-containing fragments, except for those included in the low BE peak at 284.3 eV. Accordingly, the C contents in the adsorbed fragments remaining on the surface after heating, which are evidenced by the signals in the other regions discussed so far, must be rather low.

In combination, these data indicate that at r.t. the interaction of BMP-TFSI with a Na substrate results in spontaneous decomposition of BMP, most likely into adsorbed alkyl species and tertiary amines NR_3. For the adsorbed TFSI moiety we also find significant decomposition, but in this case some of the adsorbed TFSI species are maintained either as molecularly intact adsorbates or as species where the local environment of the F, O and N atoms in TFSI is maintained. Stepwise heating of the 1.7 ML BMP-TFSI covered surface results in decomposition of the remaining TFSI-like species and of the initial decomposition products, leading to increasing formation of thermodynamically more stable binary compounds such as NaF, Na_2O, or Na_2S. Final proof for this decomposition pathway requires, however, solid identification of the different initial intermediates and final decomposition products, which is topic of the following sections.

A similar set of measurements was performed on the 8 ML BMP-TFSI film deposited at 80 K on a Na film (see Figure 2 and Figure S7). Interestingly, even upon deposition at 80 K we find some decomposition of the BMP-TFSI in direct contact with the Na surface, as indicated by the low BE peaks in the F 1s and S 2p regions after deposition of 0.2 ML BMP-TFSI. After subsequent deposition of another almost 8 ML BMP-TFSI, only the intense signals of molecularly intact BMP-TFSI were visible. The weak signals of the decomposed species directly at the interface were damped by the thick covering film and therefore below the detection limit. For this thicker film, which after deposition at 80 K was molecularly intact, one might expect that ionic liquid molecules not directly in contact with the Na surface remain intact up to higher temperatures and increasingly tend to desorb rather than to decompose. At least qualitatively, however, the measurements arrived at results essentially identical with those obtained for r.t. deposition. Also in this case, significant decomposition of the molecule ions was obtained already after annealing to r.t., and desorption and/or decomposition of the ionic liquid was completed after annealing to 420 K. Both for r.t. deposition and for deposition at 80 K and subsequent warm up to r.t. we found a high loss of N 1s intensity during annealing, indicative of significant desorption of N-containing species, while F tended to remain on the surface and form F-containing decomposition products such as NaF. Therefore, also for annealing of a thicker film reactive decomposition of BMP-TFSI is the dominant reaction pathway, while intact molecular desorption must be a minority route. Considering that in the absence of a reactive substrate such as Na the ionic liquid can be evaporated as intact molecular species (evaporator temperature in this study 470 K), this means that even for the thicker films the thermal mobility of the adsorbed species is high enough that in the range of 300 K to 400 K even ion pairs that were initially not in direct contact with the Na surface can efficiently reach this and react with it. We consider this contact layer, which is created at the interface between Na surface and ionic liquid, as the starting point of the SEI layer formed in an electrochemical environment. It is important to note that chemical interactions, without any potential effects, seem to be sufficient for its formation. Finally, one should also keep in mind that thermal desorption of metallic Na (Na multilayers) starts little above r.t.[53,54] Hence, an increasing mobility of the Na atoms may also play a role in the annealing experiments and increase the reactivity upon annealing such that at 420 K desorption/decomposition is completed.

Computational results

Intact BMP-TFSI on Na(0001)

Computationally, we first address the adsorption properties of individual, intact BMP-TFSI ion pairs on a Na surface, where we used the hcp Na(0001) surface as model (see Figure 4). This was

© 2023 The Authors. Batteries & Supercaps published by Wiley-VCH GmbH

25666223, 2023, 12, Downloaded from https://chemistry-europe.onlinelibrary.wiley.com/doi/10.1002/batt.202300336 by Cochrane Germany, Wiley Online Library on [06/12/2023]. See the Terms and Conditions (https://onlinelibrary.wiley.com/terms-and-conditions) on Wiley Online Library for rules of use; OA articles are governed by the applicable Creative Commons License

Research Article
doi.org/10.1002/batt.202300336
Chemistry Europe
European Chemical Societies Publishing

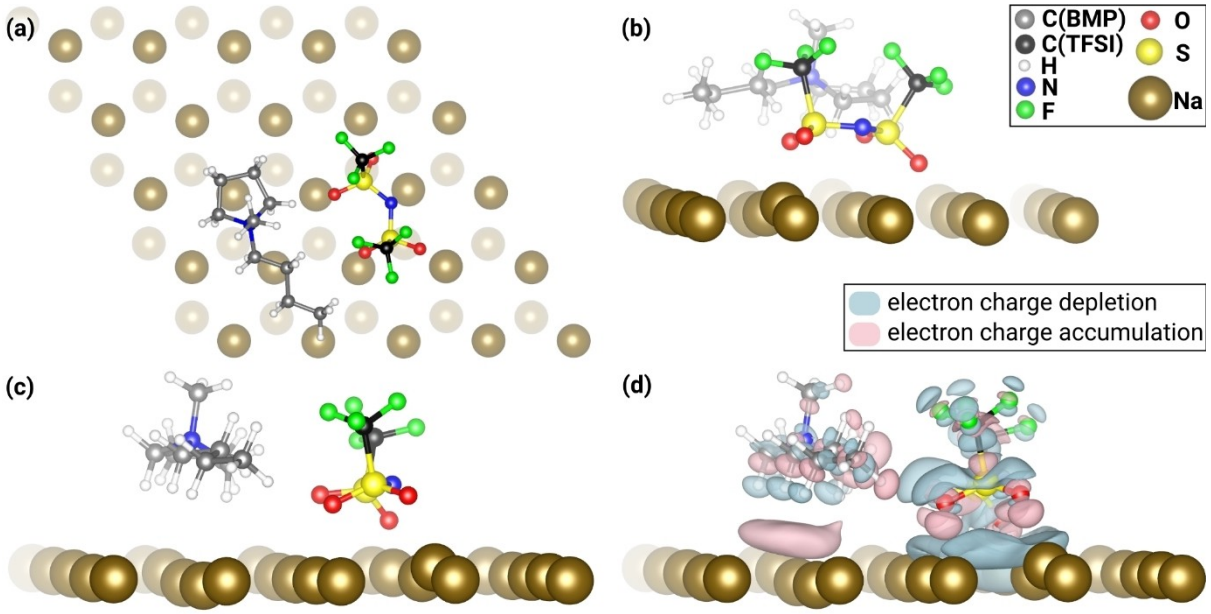

Figure 4. a) Top view and b–d) side views of the adsorption structure of BMP-TFSI within a (5×5) overlayer structure on Na(0001). In (d) the charge rearrangement due to adsorption of BMP-TFSI on Na(0001) is shown. Two isosurfaces (values of ± 0.001 e/Å^3) of the electron density difference between the electron densities of the adsorption complex and the isolated BMP-TFSI and the bare Na(0001) surface are depicted.

chosen since there are no data on the structure of multilayer Na films on Ru(0001) and since for the present calculations (at 0 K) it is the most stable surface. Here, it is important to note that test calculations using bcc Na showed very similar adsorption energies (see next section). The calculated adsorption energy of a BMP-TFSI pair in a (5×5) overlayer structure on Na(0001), where interactions between neighboring ion pairs are negligible, amounts to −1.3 eV with respect to a BMP-TFSI pair in the gas phase. TFSI adsorbs at a vertical distance of 2.9 Å between the N atom and the average position of the Na atoms in the topmost atomic surface layer. It is thus much closer to the surface than BMP, whose N atom is about 4.4 Å above the Na surface, as defined by the centers of the topmost Na layer atoms. The interaction between BMP-TFSI and the Na substrate includes different types of bonding. The contour plot of the charge rearrangement upon adsorption shown in Figure 4(d) reveals a region of enhanced charge density between Na and BMP and a region of reduced charge density between Na and TFSI. Thus, a (horizontal) dipole moment opposite to the dipole moment of the ion pair is induced in this region, pointing to significant electrostatic interactions in the adsorption complex. Furthermore, smaller regions of enhanced charge density at about 75% of the distance of the O atoms of TFSI from the nearest Na atoms (see Figure S1) hint at the formation of polar covalent bonds between these atoms, comparable to the situation on Mg(0001) (see Figure S1b). The charge rearrangement due to adsorption results in a considerable charge transfer upon adsorption. By assigning charges to the atoms according to a Bader charge analysis, about 0.6 electrons per unit cell are shifted from the Na surface to the IL, with most of it being transferred to the cation (about 0.4 electrons per unit cell). Hence, adsorption of a BMP-TFSI ion pair on Na(0001) leads to a weakening of the electrostatic interactions between the cation and anion, which goes along with emerging substrate-adsorbate interactions.

This result is very different from our previous findings for BMP-TFSI adsorption on Ag(111)[29] and HOPG (C(0001)),[30] where the two ions are about equally high above the substrate surfaces and where the charge transfer to the adsorbed ion pair was negligible. For BMP-TFSI adsorption on Mg(0001), the charge transfer to the IL ion pair was already more pronounced, but less than in the present case, and also the variation in the distance was less pronounced than for adsorption on Na-(0001).[32] Hence, we conclude an increasing contribution of covalent and (non-dynamic) electrostatic interactions in the order Ag(111) ≈ HOPG < Mg(0001) < Na(0001), for the increasingly dominant interaction between solid and TFSI. Most simply, these trends can be related to the decreasing work function of the different surfaces, which will be studied in more detail in the future.

Possible decomposition reactions of BMP-TFSI on Na(0001)

In a next step we studied the decomposition behavior of BMP-TFSI adsorbed on Na(0001), focusing on the reaction energies, which are the difference between the energies of the adsorption complexes with decomposed IL molecules and the energy of the adsorption complex with the intact BMP-TFSI. Hence, at this point we are focusing on the driving force for potential decomposition reactions, neglecting kinetic barriers. However, in a first approximation, following the Brønsted–Evans–Polanyi principle, which has been proven to hold for dissociative adsorption reactions on metal surfaces,[55] there is a

© 2023 The Authors. Batteries & Supercaps published by Wiley-VCH GmbH

25666223, 2023, 12, Downloaded from https://chemistry-europe.onlinelibrary.wiley.com/doi/10.1002/batt.202300336 by Cochrane Germany, Wiley Online Library on [06/12/2023]. See the Terms and Conditions (https://onlinelibrary.wiley.com/terms-and-conditions) on Wiley Online Library for rules of use; OA articles are governed by the applicable Creative Commons License

Research Article
doi.org/10.1002/batt.202300336
Chemistry Europe
European Chemical Societies Publishing

linear correlation between the activation energies and reaction enthalpies. Thus, comparing different reactions of similar type, the calculated reaction energies might also give a first hint on their relative probability.

Possible decomposition products, obtained by breaking a C–F (a), an S–C (b) or an N–S bond (c) of TFSI or an N–C bond of BMP (d) as well as examples of further bond breakings (e, f) are presented in Figure 5. The related reaction energies, which are given there as well, clearly demonstrate the high tendency of the adsorbed TFSI for decomposition. With a reaction energy of only about −0.7 eV for the ring opening reaction of BMP, the cation is much less prone to decomposition, comparable to the findings of previous studies.[32,33] Similar to observations on other surfaces,[30,32] energetically most favorable as initial reaction is the breaking of the N–S bond of TFSI, as the resulting decomposition products are about 0.2–0.3 eV more stable than those obtained after abstraction of a CF_3 group or of an F-atom. Breaking of both a C–F and the adjacent S–C bond (Figure 5e) further lowers the reaction energy to about −4.3 eV. Possible mixed products of BMP and TFSI decomposition are shown in Figure 5(f), where the CF_3 group of TFSI is split off and combines with an H-atom of BMP, leaving an $N(SO_2CF_3)(SO_2)$ and a tertiary N,N-dialkyl-3-buten-1-amine fragment on the surface. Yet, comparing the reaction energies of the exemplary decomposition products shown in Figure 5(e and f), suggests that breaking two bonds of the formerly TFSI ion is presumably more favorable than breaking one bond of TFSI and one bond of BMP. Yet, one should keep in mind, that entropic contributions, which might tip the balance in favor of volatile products, were not included in the calculation of the reaction energies. Experimentally, the formation and nature of volatile products might be identified by coupled gas chromatography and mass spectroscopy, such as it had been demonstrated for the reaction of BMP-TFSI and Li.[56]

Further reaction up to atomic constituents (Figure 6a) indicates that individual atoms tend to migrate into the bulk and occupy interstitial sites of the lattice, in contrast to the Mg surface (Figure 6b), where the atoms adsorb at the surface or within the topmost atomic layer.

Different from the reaction on Mg(0001), the decomposition of TFSI on Na(0001) is accompanied by a strong relaxation and restructuring of the surface atoms (see Figure 6). A quantitative comparison of the relaxation of the surface atoms of Na and Mg upon decomposition of TFSI to, in parts, atomic fragments shows a mean displacement of about 0.6 Å for Na and 0.2 Å for Mg surface atoms from their positions in the bare surfaces (see Figure S2).

Finally, we would like to note that the adsorption properties of BMP-TFSI and its initial decomposition products hardly change, if instead of hcp-Na(0001) the (100) surface of the bcc Na crystal is employed as substrate. As shown in the Supporting Information in Tables S1 and S2, the adsorption energies of intact BMP-TFSI on bcc-Na(100) and hcp-Na(0001) surfaces are essentially identical. This is also true for the adsorption energy and geometry of the adsorption complex consisting of BMP along with the two fragments NSO_2CF_3 and SO_2CF_3 of TFSI (see Table S1). Though these preliminary calculations employ only one reaction step and only two different surfaces, they indicate that the impact of the exact surface structure is presumably small.

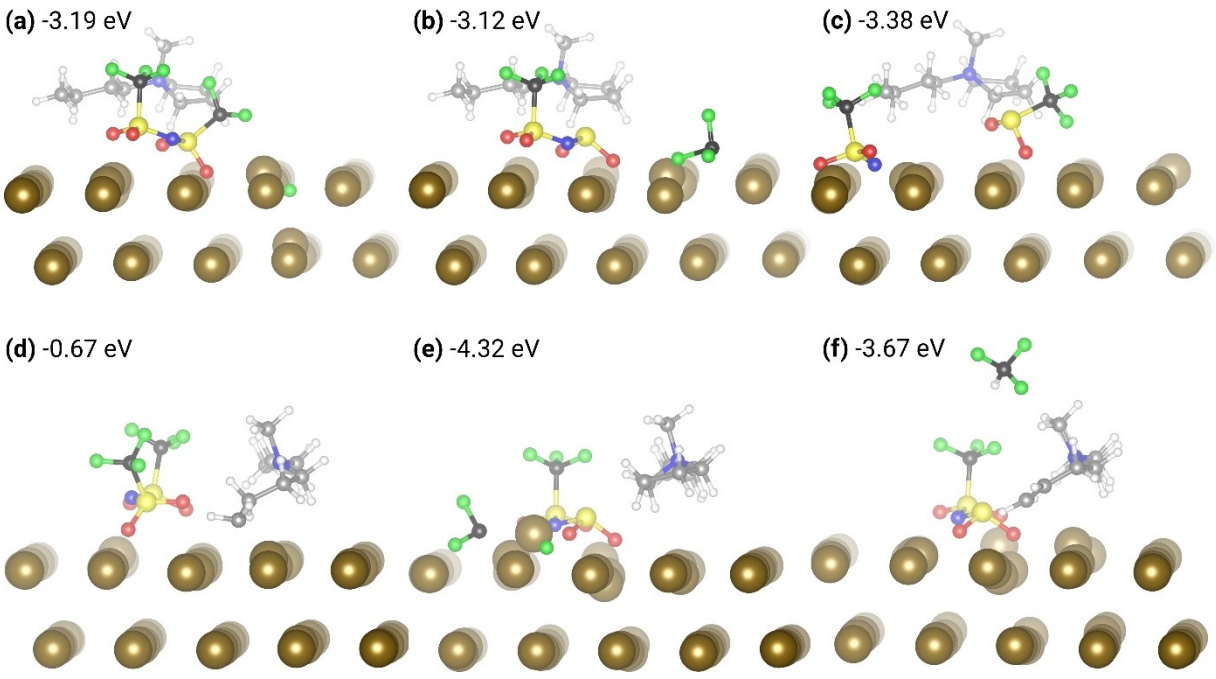

Figure 5. Structures of possible initial decomposition products of BMP-TFSI on Na(0001), obtained upon breaking a) a C–F bond, b) an S–C bond and c) an N–S bond of TFSI, or d) an N–C bond of BMP. In the decomposition product shown in panel (e), both an S–C and a C–F bond of TFSI are broken. Finally, in the structure shown in panel (f) both BMP and TFSI are decomposed and gaseous CHF_3 is formed. The respective reaction energies are given with respect to that of the intact BMP-TFSI ion pair adsorbed on Na(0001).

© 2023 The Authors. Batteries & Supercaps published by Wiley-VCH GmbH

25666223, 2023, 12, Downloaded from https://chemistry-europe.onlinelibrary.wiley.com/doi/10.1002/batt.202300336 by Cochrane Germany, Wiley Online Library on [06/12/2023]. See the Terms and Conditions (https://onlinelibrary.wiley.com/terms-and-conditions) on Wiley Online Library for rules of use; OA articles are governed by the applicable Creative Commons License

Research Article
doi.org/10.1002/batt.202300336
Chemistry Europe
European Chemical Societies Publishing

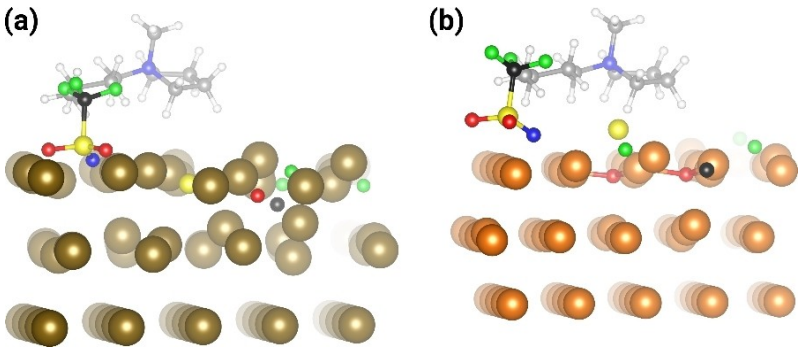

Figure 6. Structures due to further decomposition steps to, in parts, atomic adsorbates on a) the Na(0001) surface (reaction energy: −11.79 eV) and b) for comparison, the Mg(0001) surface (reaction energy: −12.35 eV).[32]

Calculated core level binding energies

Core level binding energies (BEs) were calculated both for molecularly intact adsorbed BMP-TFSI ion pairs and for selected decomposition products on Na(0001), which were identified in the previous section. The results are summarized in Table 2. Details of the calculation are described in the Computational Methods section, and also in more detail in a previous publication.[32] Most important, in our calculations the core level electron is excited to the valence state rather than into the vacuum level. Final state effects are partly included by allowing a relaxation of the valence electrons, whilst the remaining core level electrons are kept frozen. The calculated BEs were calibrated against the measured BEs for a BMP-TFSI monolayer on HOPG for each element separately.[30]

First, the calculated (and re-calibrated) core level BEs of an intact BMP-TFSI pair adsorbed on Na(0001) are given in the first row in Table 2. They differ by between +0.7 eV for the F 1s electrons and +1.3 eV for the O 1s electrons from the respective values calculated for a BMP-TFSI monolayer on graphite(0001) (HOPG).[30] Compared to the respective values of an intact BMP-TFSI pair adsorbed on Mg(0001), the calculated TFSI-related core level binding energies of BMP-TFSI on Na-(0001) are upshifted by about 0.2–0.5 eV.[32] This upshift, which would be in contrast to the overall increase in charge density on the adsorbed TFSI when going from the Mg to Na substrate, must be due to a decrease in the local charge density at the respective atoms. This agrees also with the observation that the upshift is most pronounced for the O and N atoms which are involved in the bond to Na (O) and closest to the Na substrate (O, N). The physical origin of these differences will be discussed in more detail in a forthcoming publication.

Next, we focus on possible decomposition products of BMP. For the N 1s core level of adsorbed decomposition products such as the product of the ring opening reaction (Figure 5d), or N-butyl-N-methyl-3-buten-1-amine ($N(CH_3)(C_4H_9)(C_4H_7)$) and 1-butylpyrrolidine ($N(C_4H_9)(C_4H_8)$), in the absence of co-adsorbed TFSI molecules, we calculated BEs of 400.3 eV, 400.7 eV and 400.8 eV, respectively. These values, which are about 4 eV lower than the corresponding BE of intact, adsorbed BMP-TFSI, are both close to each other and also very close to the N 1s BE of intact TFSI adsorbed on Na(0001) (400.5 eV). Therefore, they are hard to distinguish experimentally. The considerable down-shift in BE is mainly due to the fact that the adsorbed closed shell decomposition products are negatively charged by about −0.3 e^-, irrespective of the absence or presence of TFSI or its decomposition products (Figure 5f) in the supercell of the calculation. In contrast, adsorbed BMP retains about +0.5 e^- of its positive charge according to a Bader charge analysis. The adsorbed radical fragment obtained by the initial ring opening reaction (Figure 5d) is even by about −1.0 e^- negatively charged. The negative charge of the adsorbed decomposition products also affects the core levels of its carbon atoms. The C 1s BEs are downshifted by about −0.7 eV for the C_{alkyl}-atoms, between −1.3 and −1.7 eV for the C_{hetero}-atoms, and by about −3.1 eV for the terminal $C_{alkylene}$-atom bonding to the Na surface (see Figure 5d). Obviously, the most pronounced down-shifts in the BEs are observed for the two atoms involved in the N–C bond breaking process, leaving behind an unpaired and an electron lone pair on the two atoms, such that these can interact rather strongly with the Na surface. Thus, the less pronounced down-shift in the case of the other carbon atoms in the adsorbed decomposition products can be understood by the fact that they are not directly bonding to the Na surface.

Considering the closed shell decomposition products of BMP, the adsorption energies are only about −0.3 eV for the tertiary amine and about −0.5 eV for 1-butylpyrrolidine. As these adsorbed decomposition products retain no positive charge anymore, electrostatic interactions with negatively charged (decomposition products of) TFSI no longer assist the binding of the decomposition products of BMP to the substrate and thus desorption is expected to take place already at relatively low temperatures.

In total, decomposition of adsorbed BMP can lead to adsorbed products that are partly negatively charged, with N 1s BEs similar to each other and to that in TFSI.

Looking at TFSI, its largest and thus structurally most similar decomposition product is obtained by abstracting an F-atom. The remaining adsorbed $N(SO_2CF_3)(SO_2CF_2)$ species (see Figure 5a) interacts, like intact TFSI, via the O atoms with the Na surface. Additionally, the N-atom gets much closer to the surface, enabling direct Na–N interactions. This can explain the decrease of the N 1s BE of the adsorbed $N(SO_2CF_3)(SO_2CF_2)$ fragment by about 0.9 eV compared to the respective BE within

© 2023 The Authors. Batteries & Supercaps published by Wiley-VCH GmbH

25666223, 2023, 12, Downloaded from https://chemistry-europe.onlinelibrary.wiley.com/doi/10.1002/batt.202300336 by Cochrane Germany, Wiley Online Library on [06/12/2023]. See the Terms and Conditions (https://onlinelibrary.wiley.com/terms-and-conditions) on Wiley Online Library for rules of use; OA articles are governed by the applicable Creative Commons License

Research Article
doi.org/10.1002/batt.202300336

Chemistry Europe
European Chemical Societies Publishing

Table 2. Computed core level binding energies (in eV) of adsorbed BMP-TFSI ion pairs and possible decomposition products in a (5×5) overlayer structure on Na(0001). The structures of the decomposition products listed in rows 1–8 are shown in Figures 5 and 6(a), structures of the other adsorbed fragments listed in rows 10–29 are shown in Figures S3–S6 in the Supporting Information. Most atomic adsorbates occupy octahedral interstitial sites of the Na(0001) slab (oct), only F adsorbs in a hollow position on Na(0001). Note that in the topmost part, up to the BMP-based adsorbed fragments, all energies were calculated in the presence of both ions or their fragments, whereas in the lower parts only the respective adsorbates were considered.

	N 1s	S 2p	O 1s	C 1s	F 1s
BMP-TFSI	400.5 (N_{TFSI}) 404.3 (N_{BMP})	169.7	534.1	293.5 (C_{TFSI}) 288.9 ($C_{BMP/hetero}$) 287.3 ($C_{BMP/alkyl}$)	689.8
BMP-$N(SO_2CF_3)(SO_2CF_2)$-F	404.2 (N_{BMP}) 399.6	169.5 (SO_2CF_3) 168.1 (SO_2CF_2)	533.7; 533.8 (SO_2CF_3) 533.4; 533.5 (SO_2CF_2)	288.3 (SO_2CF_2)	689.6 (SO_2CF_3) 688.2 (SO_2CF_2) 684.9 (F)
BMP-$N(SO_2CF_3)(SO_2)$-CF_3	404.3 (N_{BMP}) 399.4 ($NSO_2CF_3SO_2$)	169.3 (NSO_2CF_3) 167.3 (SO_2)	533.7 (SO_2CF_3) 532.8 (SO_2)	293.3 (SO_2CF_3) 289.8 (CF_3)	689.6 (SO_2CF_3) 687.2 (CF_3)
BMP-NSO_2CF_3-SO_2CF_3	404.3 (N_{BMP}) 397.7 (NSO_2CF_3)	168.3 (NSO_2CF_3) 166.7 (SO_2CF_3)	532.7 (NSO_2CF_3) 532.8 (SO_2CF_3)	292.8(NSO_2CF_3) 292.5 (SO_2CF_3)	689.2(NSO_2CF_3) 689.5(SO_2CF_3)
$N(CH_3)(C_4H_9)(C_4H_8)$-TFSI	400.3 400.4 (N_{TFSI})	169.7	534.0	287.2-287.6 ($C_{BMP/hetero}$) 286.6 ($C_{BMP/alkyl}$) 286.0 ($C_{BMP/alkylene\text{-}chain}$) 284.2 ($C_{BMP/alkylene\text{-}terminal}$)	689.8
BMP-$N(SO_2CF_3)SO_2$-CF_2-F	399.4	169.3 (SO_2CF_3) 167.2 (SO_2)	532.8 (SO_2)	293.2 (SO_2CF_3) 285.9 (CF_2)	689.5 (SO_2CF_3) 686.3; 686.6 (CF_2) 684.9 (F)
$N(CH_3)(C_4H_9)(C_4H_7)$-$N(SO_2CF_3)(SO_2)$-CHF_3	400.7 399.4	169.3 (SO_2CF_3) 167.1 (SO_2)	533.7 (SO_2CF_3) 532.9 (SO_2)	293.3 (SO_2CF_3)	689.9 (CHF_3) 689.6 (SO_2CF_3)
BMP-NSO_2CF_3-S-2O-C-3F	404.3 (N_{BMP}) 397.8 (NO_2CF_3)	168.5 (NSO_2CF_3) 160.5 (S)	532.8; 532.9 (NSO_2CF_3) 528.4; 528.5 (O)	292.9 (NSO_2CF_3) 282.5 (C)	689.3 (NSO_2CF_3) 684.8; 685.0 (F)
BMP based adsorbed fragments					
BMP	404.3				
$N(CH_3)(C_4H_9)(C_4H_7)$	400.7				
$N(C_4H_9)(C_4H_8)$	400.8				
TFSI based adsorbed fragments					
NSO_2F	397.6	168.5	532.7		686.6
NSO_2	395.9	165.3	530.6		
NSO	396.4	163.7	530.9		
SO_2		164.1	531.3		
Diatomic adsorbed fragments					
CN	398.5			285.4	
SN	395.8	161.6			
SC		161.3		283.2	
SO		161.8	530.5		
S_2		161.0			
O_2			529.9		
Monatomic adsorbed fragments					
N (oct)	394.5				
S (oct)		160.4			
O (oct)			528.6		
C (oct)				282.5	
F (ad hollow) F (oct)					684.4 684.8

© 2023 The Authors. Batteries & Supercaps published by Wiley-VCH GmbH

25666223, 2023, 12, Downloaded from https://chemistry-europe.onlinelibrary.wiley.com/doi/10.1002/batt.202300336 by Cochrane Germany, Wiley Online Library on [06/12/2023]. See the Terms and Conditions (https://onlinelibrary.wiley.com/terms-and-conditions) on Wiley Online Library for rules of use; OA articles are governed by the applicable Creative Commons License

an intact, adsorbed BMP-TFSI pair. Substantial changes are observed also in the core level BEs of the SO_2CF_2 subgroup (down-shifts of 0.6 eV (O 1s), 1.6 eV (S 2p, F 1s), 5.2 eV (C 1s)). The removal of a strongly electronegative F atom in the CF_3 group results in a considerable charge rearrangement within the SO_2CF_2, which is most pronounced for the neighboring carbon atom. In contrast, hardly any changes are found in the core level BEs of the SO_2CF_3 subgroup of the fragment which are only down-shifted by 0.2–0.4 eV. Qualitatively, this latter trend can be understood by a similar binding situation and thus local environment of this subgroup in the adsorbed decomposition product and in the adsorbed BMP-TFSI pair.

The same SO_2CF_3 subgroup is also present in the fragment $N(SO_2CF_3)(SO_2)$, which is obtained when a CF_3 group is abstracted from TFSI, and also in this case the down-shifts of the core level BEs relative to the BE in adsorbed BMP-TFSI are rather small. In contrast, for the SO_2 subgroup of $N(SO_2CF_3)(SO_2)$, the down-shifts in the O 1s (−1.3 eV) and S 2p (−2.4 eV) BEs are significant. This can easily be rationalized since here the electron withdrawing CF_3 group is missing and additional electronic charge is shifted from the N-atom that is bound to the Na surface to the SO_2 group. Such effect was already described for the same decomposition product of TFSI on Mg(0001).[32] If the abstracted CF_3 or CF_2 group persists as adsorbate on the surface and does not desorb, as assumed in our calculations and shown in Figure 5(b and e), the C 1s and F 1s BEs of these groups are down-shifted by about −3.7 eV to −7.6 eV (C 1s) and −2.6 to −3.5 eV (F 1s) compared to the respective values within the intact TFSI adsorbate. Also this can easily be understood by assuming a significant direct charge transfer from Na to the C and also F atoms in these adsorbed groups as compared to the situation in adsorbed TFSI.

By breaking one N–S bond of the adsorbed TFSI moiety, the two adsorbed fragments NSO_2CF_3 and SO_2CF_3 are obtained, in which the Na–O bonds are retained and a new, additional bond between the Na surface and the N-atom of the fragment NSO_2CF_3 is formed. As shown in the previous section, this is the thermodynamically most stable initial decomposition product. With the formation of the Na–N bond, additional charge is transferred from the Na surface to the adsorbed species, causing a substantial lowering of the N 1s, S 2p and O 1s BEs of this fragment compared to the respective values of intact, adsorbed TFSI. The resulting down-shifts of the BEs are −2.8 eV for the N 1s state and −1.4 eV for the S 2p and O 1s states. The impact on the C 1s and F 1s core level binding energies is much smaller ($\Delta BE = -0.7$ and −0.6 eV, respectively), most likely, as these atoms are not directly involved in the bond breaking and formation processes.

Similar N 1s, S 2p and O 1s BEs as in the adsorbed NSO_2CF_3 fragment are also observed for the adsorbed fragment NSO_2F, which can be obtained by removal of a CF_2 group. In contrast, the F 1s BE (686.6 eV) is significantly lower than in adsorbed TFSI or in the adsorbed NSO_2CF_3 fragment. A comparable change in the F 1s BE was already observed in a similar study of TFSI and NSO_2F adsorption on Mg(0001),[32] and attributed to the change from the F_2C–F bond to an O_2S–F bond. Thus, the CF_2 group with the two highly electronegative F atoms is replaced by a less electronegative SO_2 group as neighbor to the remaining F atom in this species.

The core level BEs of the other adsorbed fragment obtained by the cleavage of the N–S bond of TFSI (SO_2CF_3 fragment) differ by less than 0.3 eV from the respective values of the NSO_2CF_3 fragment, except for the S 2p core level binding energy, which is about −1.6 eV lower. This latter down-shift might be explained by an additional charge transfer from the Na surface to the SO_2CF_3 fragment, which accumulates on the S-atom of the fragment. The charge increase is reflected by an increase of the number of electrons within the Wigner–Seitz radius of the S atom by about 0.013 electrons. For comparison, the Bader charge of the S atom within adsorbed SO_2CF_3 is about −1 electron smaller compared to its value in adsorbed NSO_2CF_3 adsorbed.

Continuing the decomposition of the adsorbed TFSI species, removal of the electronegative F atom from the NSO_2F fragment leads to an adsorbed sulfonyl imide species (NSO_2), which is also energetically favorable.[32] This results in a further, considerable down-shift of the S 2p, N 1s and O 1s BEs ($\Delta BE = -3.2$ eV; −1.7 eV and −2.1 eV). Apparently, removal of the F atom affects not only the direct neighbors, but also second nearest neighbor atoms. Due to the S–F bond breaking, the electronic structure within NSO_2 rearranges and stronger Na–N and Na–O bonds can be formed, as revealed by about 0.1 Å shorter Na–N and Na–O distances (see Figure S4) Further reduction of the sulfonyl imide to adsorbed thiazate (NSO) or to a sulfurdioxyl (SO_2) fragment lowers the S 2p BE by another −1.6 eV or −1.2 eV, respectively, resulting in total shifts of −6.0 or −5.6 eV compared to intact adsorbed TFSI. The N 1s and O 1s BEs of the adsorbed NSO and SO_2 fragments are slightly higher than in the NSO_2 fragment (ΔBE(N 1s): +0.5 eV, ΔBE-(O 1s): +0.3 eV, +0.9 eV). Due to the removal of the N atom or of an O atom from NSO_2, additional charge accumulates at the S atom of the NSO and at the SO_2 fragments, which not only stems from the Na surface but is also taken from the remaining bonding partners, leading to a slight increase in charge at the remaining O- or N-atoms.

Smaller, diatomic fragments, studied herein mainly adsorb within the first surface layer of Na atoms or partly occupy interstitial sites of the Na(0001) slab (see Supporting Information, Figure S5). For sulfur containing diatomic compounds, such as S_2, SC, SN and SO, the S 2p binding energies are in the range of 161.0–161.8 eV (Table 2). As expected, the more electronegative the binding partner, the higher the S 2p BE. For the diatomic cyanide molecule adsorbed on Na, we find a different hybridization of the atomic orbitals compared to the fragments discussed so far. Hence, the N 1s and C 1s BEs are also not directly comparable to any of the values discussed so far, but about −2 eV and −8.1 eV lower than in intact, adsorbed BMP-TFSI. Yet, the values are comparable to the respective values for other cyanides.[33]

Finally, as discussed in the previous section, most of the studied atomic adsorbates tend to migrate into the Na subsurface region and occupy interstitial subsurface sites of the Na(0001) surface (see Figure 6 and Supporting Information, Figure S6). A closer study of atomic adsorption at a coverage of

© 2023 The Authors. Batteries & Supercaps published by Wiley-VCH GmbH

25666223, 2023, 12, Downloaded from https://chemistry-europe.onlinelibrary.wiley.com/doi/10.1002/batt.202300336 by Cochrane Germany, Wiley Online Library on [06/12/2023]. See the Terms and Conditions (https://onlinelibrary.wiley.com/terms-and-conditions) on Wiley Online Library for rules of use; OA articles are governed by the applicable Creative Commons License

Research Article
doi.org/10.1002/batt.202300336
Chemistry Europe
European Chemical Societies Publishing

1 adatom per 25 Na surface atoms confirms the preferred subsurface adsorption sites, except for F atoms, which preferentially adsorb in a hollow position at the surface. Note that in this case, different from Figure 6, the adsorption energy was calculated without any other co-adsorbed BMP or TFSI fragments (see Supporting Information, Figure S6). The BEs of the adsorbed species are considerably down-shifted compared to the BEs in the intact, adsorbed BMP-TFSI ion pair on Na(0001), by −11.0 eV (C 1s), −9.3 eV (S 2p), −5.9 eV (N 1s), −5.5 eV (O 1s) and −5.4 eV (F 1s) respectively. This trend fully agrees with expectations, as one would expect a considerable charge transfer from Na atoms to the atomic adsorbates (formation of Na–X bonds) as compared to the situation in molecular TFSI. On the other hand, compared to the BEs of the respective atomic adsorbates on Mg(0001), the BEs on Na(0001) are about the same (C 1s) or down-shifted by −0.5 eV (S 2p), −1.5 eV (N 1s) and −2 eV (O 1s, F 1s). This latter trend can be rationalized by the increasing electronegativity of the elements C < S < N < O < F, which leads to an increase in the charge transfer. This charge transfer is more pronounced for Na compared to Mg as the alkali metal is more electropositive.

In total, we obtained a comprehensive set of BEs for a variety of different possible decomposition products, which were selected based on their energetic stability.

Comparison of experimental and calculated core level binding energies of decomposition products

Finally, we tried to identify the reaction products of BMP-TFSI and Na by comparison of the calculated and measured BEs. In Figure 7 we show the XP spectra recorded after deposition of 1.7 ML BMP-TFSI at r.t. on the Na film together with symbols marking the calculated BEs of the ions or their possible decomposition fragments as given in Table 2. These spectra were chosen for comparison as they include most of the peaks that are observed in the series of spectra shown in Figure 3. However, we would like to point out that upon thermal treatment there seems to be a rigid downshift of the spectra by about 1 eV.

In all spectral ranges the high BE peaks can be explained by core level electrons of adsorbed, intact TFSI. Here, one should

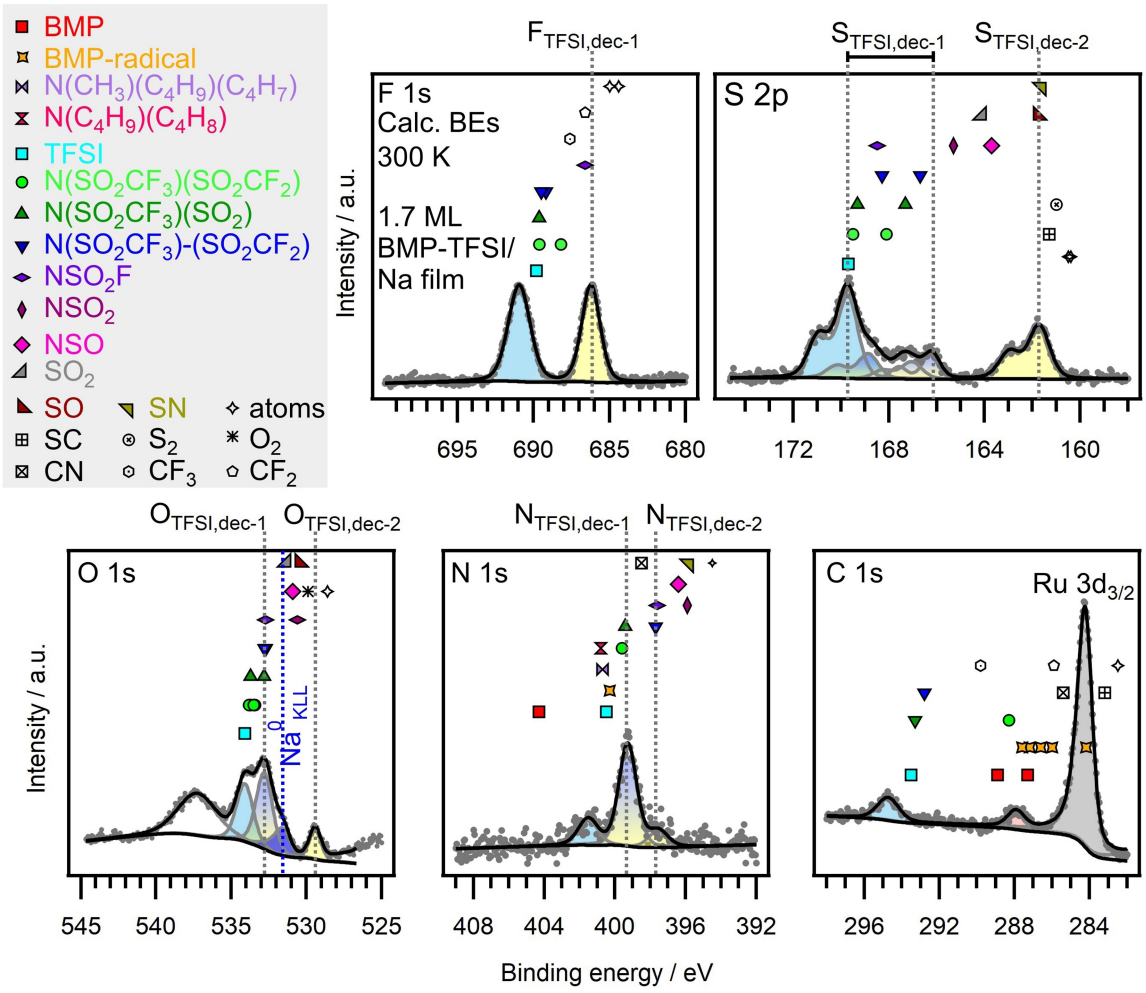

Figure 7. Comparison of experimental XP spectra measured on a 1.7 ML BMP-TFSI film deposited on a Na film at r.t. (see also Figure 3) and calculated core level binding energies of the fragments shown in Table 2 (colors see Figure 3). The calculated BEs do not relate to the intensity axis, but have been inserted at different vertical positions for reasons of clarity.

© 2023 The Authors. Batteries & Supercaps published by Wiley-VCH GmbH

25666223, 2023, 12, Downloaded from https://chemistry-europe.onlinelibrary.wiley.com/doi/10.1002/batt.202300336 by Cochrane Germany, Wiley Online Library on [06/12/2023]. See the Terms and Conditions (https://onlinelibrary.wiley.com/terms-and-conditions) on Wiley Online Library for rules of use; OA articles are governed by the applicable Creative Commons License

keep in mind that the high BE peak appearing at around 538 eV in the O 1s region is related to a Na-related Auger process. Considering the possible initial decomposition fragments N-(SO_2CF_3)(SO_2), N(SO_2CF_3) and SO_2CF_3, all of them are possible reaction intermediates, as the experimental spectra contain peaks that would be consistent with the positions of their calculated BEs. Specifically, the calculated F 1s, S 2p, O 1s and C 1s BEs of the SO_2CF_3 subgroup of the fragment N(SO_2CF_3)(SO_2) are close to the respective calculated and experimental BEs of intact, adsorbed TFSI and thus can contribute to the measured signals associated with the TFSI group. For the N 1s signal, the BE calculated for N(SO_2CF_3)(SO_2) fits well to the most intense peak in the N 1s regime ($N_{TFSI,dec-1}$). Moving on to the N(SO_2CF_3) and SO_2CF_3 fragments, their calculated F 1s and C 1s BEs approximately coincide with the high BE peak of the respective regions in the experiment. Furthermore, the S 2p, O 1s and N 1s BEs of N(SO_2CF_3), SO_2CF_3 and of the SO_2 subgroup of N(SO_2CF_3)(SO_2) agree with the positions of the peaks $S_{TFSI,dec-1}$, $O_{TFSI,dec-1}$ and $N_{TFSI,dec-1}$ in the experimental data.

On the other hand, we can exclude decomposition of the adsorbed TFSI by abstracting an F atom, forming N-(SO_2CF_3)(SO_2CF_2), although a number of the calculated BEs would be consistent with the experimental spectra. This exclusion is based on the fact there is no peak in the experimental spectrum at or close to the position of the calculated BE of the F 1s electron of the SO_2CF_2 group (688.2 eV), which is in the minimum between the two experimental peaks.

As stated already in the previous section, the N 1s BEs of possible decomposition products of BMP, such as the N,N-dialkyl-buten-amine or 1-butylpyrrolidine, are comparable to those of intact adsorbed TFSI und hence these products would contribute to the high BE peak in the N 1s regime of the experimental spectrum. It could only be distinguished from intact adsorbed TFSI by a complete quantitative analysis of all spectra, which due to the unknown contributions of TFSI decomposition products is hardly possible.

The peaks at low BEs in the F 1s, S 2p and O 1s experimental spectra are slightly higher in BE than the corresponding calculated BEs of adsorbed atoms. Nevertheless, as the peaks in the experimental spectra are downshifted after annealing, we tentatively attribute those peaks in the experimental spectra to adsorbed F, S and O atoms. Hence, parts of the adsorbed TFSI ions and/or its fragments decompose down to the respective atomic constituents upon deposition at r.t. For N, the situation is different, as no peak in the range of adsorbed N atoms on Na (calculated N 1s BE: 394.5 eV) is observed. Furthermore, we like to note, that the BEs of the respective binary bulk compounds NaF, Na_2S or Na_2S_2 and Na_2O were reported to be in the same range[37,45–47] as the calculated BEs of the atoms adsorbed on Na. Thus, a progressing formation of the binary compounds might also occur.

For the S 2p regime, the low BE peak would also be consistent with the adsorbed diatomic fragments S_2 or SC, and also with SO and SN. Formation of the latter two species can, however, be excluded, as there are no peaks in the experimental spectra at the position of their calculated N 1s or O 1s BEs.

The low BE peak in the F 1s regime might also be related to adsorbed NSO_2F or CF_2 fragments, as their calculated BEs are only by about 0.6 eV higher than the peak in the experimental spectra. Yet, as the calculated BE of intact TFSI or large fragments were underestimated by about 1 eV compared to the experiment and keeping in mind, that the experimental spectrum down-shifts upon heating, we tend to exclude NSO_2F and CF_2 as observable intermediate products, although for adsorption on Mg they were calculated to be energetically possible.[32]

Other small fragments, such as NSO_2, NSO, SO_2, CF_3 or O_2 can be ruled out, as no peak is observed close to the calculated N 1s BE of NSO_2 or NSO, the calculated S 2p BE of SO_2, the calculated F 1s BE of CF_3 or the calculated O 1s BE of inserted O_2 (see Figure S5f).

To sum up, in all spectral ranges the peaks (S 2p, O 1s, N 1s, F 1s) at highest BEs are consistent with core levels of intact TFSI or of the decomposition products of BMP (N,N-dialkyl-buten-amine, 1-butylpyrrolidine) or TFSI (N(SO_2CF_3), N(SO_2CF_3)(SO_2)). The calculated BEs of the latter two decomposition products also agree with the peaks $S_{TFSI,dec-1}$, $O_{TFSI,dec-1}$ and $N_{TFSI,dec-1}$ observed experimentally. On the other hand, the peaks at low BEs in the F 1s, S 2p and O 1s regimes can be attributed to adsorbed atoms or to the respective binary compounds NaF, Na_2S or Na_2S_2 and Na_2O. Formation of the latter species is postulated at higher coverages of BMP-TFSI.

Consequently, we suggest that upon interaction with Na^0, the BMP cation decomposes to alkylpyrrolidine or tertiary amine compounds, which based on their low adsorption energies (see previous section) are expected to desorb at elevated temperatures according to Reaction (1):

$$\begin{aligned} &BMP_{ad} \rightarrow N(C_4H_9)(C_4H_8)_{ad} + CH_{3,ad} \\ &\xrightarrow{\Delta} N(C_4H_9)(C_4H_8)\uparrow + {}^1\!/_2\ C_2H_6\uparrow \end{aligned} \quad (1)$$

In parallel, the adsorbed TFSI anion eventually decomposes to N(SO_2CF_3) and atomic S, F and O fragments on the Na surface, after passing through larger fragments, as indicated by Reaction (2):

$$\begin{aligned} &TFSI_{ad} \rightarrow (N(SO_2CF_3)(SO_2)_{ad} + 3\ F_{ad} + C_{ad} \rightarrow) \\ &N(SO_2CF_3)_{ad} + 3\ F_{ad} + 2\ O_{ad} + S_{ad} + C_{ad} \end{aligned} \quad (2)$$

In addition, also mixed products resulting from the simultaneous decomposition of both adsorbed ions are possible (see Figure 5f), as indicated by Reaction (3):

$$\begin{aligned} &BMP\text{-}TFSI_{ad} \rightarrow \\ &N(CH_3)(C_4H_9)(C_4H_7)_{ad} + N(SO_2CF_3)(SO_2)_{ad} + CHF_3 \end{aligned} \quad (3)$$

Similar decomposition reactions have been also deduced from model studies of BMP-TFSI adsorption on Mg or reactions of BMP-TFSI and Li,[32,33] indicating that these chemical decomposition pathways are characteristic for the chemical interaction of BMP-TFSI with highly electropositive metal surface.

© 2023 The Authors. Batteries & Supercaps published by Wiley-VCH GmbH

25666223, 2023, 12, Downloaded from https://chemistry-europe.onlinelibrary.wiley.com/doi/10.1002/batt.202300336 by Cochrane Germany, Wiley Online Library on [06/12/2023]. See the Terms and Conditions (https://onlinelibrary.wiley.com/terms-and-conditions) on Wiley Online Library for rules of use; OA articles are governed by the applicable Creative Commons License

Here, we would like to emphasize that these decomposition reactions were identified as a result of purely chemical interactions between BMP-TFSI and the Na surface, in the absence of an applied electrical field and related charging effects. Hence, these results can be considered as characteristic for the initial phase of the chemical formation of a solid electrolyte interphase. Comparing with an electrochemistry experiment, this should be most closely related to the behavior under open circuit conditions. While electric field/charging effects may modify some aspects of the decomposition pattern of BMP-TFSI interacting with a Na surface, the rather high reaction energies obtained for the chemical decomposition clearly indicate that these chemical interactions contribute strongly if not predominantly to the Na-induced decomposition of BMP-TFSI. On the other hand, other effects that could occur in an electrochemical environment, such as a layering of the ionic liquid, due to surface charging,,[57–60] or interactions with charged shuttle ions were not included here and have to be treated separately.

Finally, we would like to comment on the applicability and relevance of the present findings for real systems. We believe that the results obtained here for a highly idealized system properly identify the trends governing BMP-TFSI decomposition in contact with metallic Na, in the very initial stage of the SEI formation. This includes both the chemical driving force and, on a qualitative scale, activation barriers. Metallic Na may be present not only in the case of bulk Na anodes, but also as thin layers during Na deposition (Na plating) on host anode materials such as hard carbon. The good agreement with realistic systems is indicated, e.g., by the fact that already at room temperature significant amounts of NaF or closely related F-containing compounds are formed in the model system (see Figure 3), in good agreement with previous reports on SEI formation in realistic systems.[23] Conclusions on aspects such as the mechanisms dominating the ongoing growth of the SEI, including transport processes, are, in contrast, not possible from our findings. The same is also true for cation effects, such as the interaction of Na^+ cations with BMP-TFSI decomposition products, while BMP-TFSI ion pairs seem to be stable with respect to Na^+. Overall, this work provides detailed insights into the initial stages of SEI formation in SIBs that are hardly available from a realistic system.

Conclusions

The reactive interaction between the ionic liquid BMP-TFSI and a Na surface was studied by XPS experiments, involving vapor deposition of thin BMP-TFSI films on a Na surface, and DFT calculations. While at 80 K, BMP-TFSI adsorbs molecularly intact on oxygen-free metallic Na thin films, we find immediate partial decomposition of adsorbed BMP-TFSI upon deposition at or annealing to r.t. Decomposition is further activated upon subsequent thermal treatment. Complete removal of molecularly intact BMP-TFSI is reached upon annealing to 420 K. Since this is still below the desorption temperature of molecular BMP-TFSI, reactive decomposition must prevail, while desorption of molecularly intact BMP-TFSI plays a very minor role. Furthermore, the complete disappearance of molecularly intact BMP-TFSI indicates that not only the BMP-TFSI layer in direct contact with the Na surface undergoes reactive decomposition, but also higher layers, which points to considerable mobility at the interface under these conditions, at temperatures between <300 K and 420 K. This includes both mobility of Na surface atoms and of the molecular ions and decomposition products of BMP-TFSI. Further stepwise annealing up to 570 K results in progressing decomposition, up to the level of adsorbed elemental species (F_{ad}, O_{ad}, S_{ad}) or the respective binary compounds (NaF, Na_2O, Na_2S). The considerable intensity loss of the different elemental signals indicates the formation and subsequent desorption of volatile reaction products, which is particularly pronounced for N-containing species. Possible decomposition pathways are identified by the calculated stability of the resulting reaction products and by comparison between calculated binding energies and the measured spectra recorded after deposition and after subsequent annealing steps. Besides the thermodynamically stable atomic fragments of TFSI on the Na surface, larger fragments of the ions such as $N(SO_2CF_3)$, $N(SO_2CF_3)SO_2$ or N,N-dialkyl-3-buten-1-amine or 1-butylpyrrolidine are formed, depending on the experimental conditions. Weakly bound, neutral decomposition products of BMP desorb upon formation at elevated temperatures. The decomposition pathways described above can be considered as characteristic for the first steps of a chemical formation of a solid electrolyte interphase (SEI) at the interface between the ionic liquid and a Na surface. Furthermore, the rather strong interactions between Na and the BMB-TFSI decomposition products point to the formation of a homogeneous layer at the interface at this stage.

Overall, this works further demonstrates the potential of combined calculational and experimental studies of well-defined model systems for providing detailed, molecular scale insights into the complex electrolyte decomposition reactions and the composition of the products. This is a prerequisite for the systematic knowledge-based development of electrolytes with tailored stabilities and decomposition patterns that are indispensable for an improved battery performance.

Methods

Experimental methods

The experiments were carried out in a commercial UHV system (SPECS) with a base pressure of 2×10^{-10} mbar. It consists of two chambers, one containing an Aarhus-type STM/AFM system (SPECS Aarhus SPM150 with a Colibri sensor), the other one is equipped with an X-ray source (SPECS XR50, Al–K_α and Mg–K_α), a He lamp (SPECS UVS 300) and a hemispherical analyzer (SPECS, DLSEGD-Phoibos-Has3500) for XPS and UPS measurements.

The Ru(0001) single crystal (one side polished, orientation accuracy of $<0.1°$) was purchased from MaTecK. A clean and smooth Ru(0001) substrate was prepared by repeated cycles of Ar^+ ions sputtering (1 keV) and subsequent flash heating to ~1700 K,

© 2023 The Authors. Batteries & Supercaps published by Wiley-VCH GmbH

25666223, 2023, 12, Downloaded from https://chemistry-europe.onlinelibrary.wiley.com/doi/10.1002/batt.202300336 by Cochrane Germany, Wiley Online Library on [06/12/2023]. See the Terms and Conditions (https://onlinelibrary.wiley.com/terms-and-conditions) on Wiley Online Library for rules of use; OA articles are governed by the applicable Creative Commons License

followed by O_2 adsorption at temperatures below 500 K. At the end of the preparation procedure the sample was flashed to 1700 K to remove remaining adsorbed oxygen.[61]

The ionic liquid (IL) 1-butyl-1-methylpyrrolidinium bis(trifluoromethylsulfonyl)imide (BMP-TFS, Merck, ultrapure) was filled into a quartz crucible of a triple Knudsen effusion cell (Ventiotec, OVD-3). Prior to its use, the IL was purified by careful degassing, first briefly in the load lock and then under ultrahigh vacuum (UHV) conditions at around 400 K for 24 h, where the pressure increase from the base pressure was negligible. This way we obtained a pure, water-free IL. For deposition of IL adlayers on Ru(0001) and on the thin Na films, respectively, we evaporated the IL at an IL source temperature of 470 K (pressure increase $<1\times10^{-10}$ mbar). Under these conditions the deposition rate was ~0.1 ML min^{-1}, with 1 ML defined as a layer at saturation coverage (approx. layer thickness of 3.5 Å). This also means that at room temperature the deposited film is kinetically stabilized and IL desorption can be neglected. Sodium metal was deposited from an alkali getter source (SAES Getters), by resistively heating the source (7.5 A, 1.4 V) in line-of-sight of the sample (distance getter source – sample in the range of a few cm).

The layer thickness d of the Na thin films and of the adsorbed BMP-TFSI was derived from the damping of the Ru 3d ($3d_{3/2}$: 284.3 eV and $3d_{5/2}$: 280.1 eV) electron intensities, using the relation $d=-\ln(I_d/I_0)\times(\lambda\cos\theta)$ (I_0: substrate peak intensity before deposition, I_d: intensity after deposition, λ: the inelastic mean free path (IMFP) in the film material at this electron energy, θ: emission angle with respect to the surface normal). For the Ru $3d_{5/2}$ electrons with a kinetic energy of around 1207 eV we used values of 46.7 Å[62] and 35.4 Å[63] for λ_{Na} and $\lambda_{BMP\text{-}TFSI}$, respectively. This evaluation assumes a homogeneous growth of the Na film, which considering previous reports seems to be reasonable. Therefore we expect the resulting values to be reasonably reliable (within ±15%).

The XP spectra were recorded using monochromatized Al Kα radiation ($h\nu_0=1486.6$ eV) at a power of 400 W ($U=15$ kV, $I=26.7$ mA), with a pass energy of 20 eV for all detail spectra. All spectra were recorded at electron emission angles of 0° and 70° with respect to the surface normal. In normal emission (0°) the measurement is sensitive to the extended surface region (information depth (ID) around 60–90 Å), at grazing emission (70°) to the near surface region (ID around 10–30 Å). Peak fitting was performed using the Igor pro 8.04 software; all peaks were fitted with a simultaneous fit of the background (Shirley+slope) and signal, assuming a pseudo-Voigt type peak shape, which is a linear combination of a Gaussian and a Lorentzian function. The binding energy (BE) scale was calibrated by setting the position of the Ru $3d_{5/2}$ peak to 280.1 eV.

For the UPS measurements (He I: $h\nu=21.2$ eV) we applied a bias voltage of −5.0 V to the sample to accelerate the photoelectrons into the analyzer (pass energy $E_{pass}=1$ eV). Here, the energy scale was adjusted such that the intensity increase at the Fermi level (EF) defines the zero point (0 eV BE). The position of the Fermi level was determined from the UPS spectrum of a Ru(0001) crystal.

Computational methods

Periodic density functional theory (DFT) calculations, which are well suited to tackle basic battery-relevant problems,[64] were performed to elucidate the adsorption and possible reactions of BMP-TFSI on Na surfaces. We employed the Vienna ab initio simulation package (VASP 5.4).[65,66] The electron-ion interaction was described by the projector augmented wave (PAW) method.[67,68] Pursuant to detailed benchmark studies (see Supporting Information, Tables S1–S3) the Na PAW potential including one valence electron was chosen. Electron exchange and correlation were treated within the generalized gradient approximation, employing a revised version of the Perdew–Burke–Ernzerhof functional (RPBE).[69] Dispersion effects were accounted for by a semiempirical correction scheme proposed by Grimme (D3),[70] damped as proposed by Chai and Head–Gordon.[71] The electronic wave functions were expanded in a plane wave basis set up to a cutoff energy of 520 eV. In all calculations the electronic structure was converged within 10^{-6} eV.

The Na(0001) surface was modelled by a slab of three atomic layers separated by a vacuum region of about 28 Å. A (5×5) supercell of the surface unit cell is used for adsorption structures of a BMP-TFSI pair on Na(0001). For the integration over the first Brillouin zone a (2×2×1) *k*-point mesh was employed.

For all geometry optimizations the two uppermost atomic layers of the surface slab were allowed to relax, whilst the lowest layer was fixed to imitate bulk like behavior. Geometry optimizations were carried out until all forces on atoms were less than 0.01 eV/Å. In the evaluation of dispersion energies only atoms of BMP-TFSI and the Na atoms of the topmost layer were included. Dispersion interactions between Na atoms were disregarded.

Adsorption energies E_{ad} were calculated according to Equation (4):

$$E_{ad} = E(\text{adsorption complex}) - E(\text{Na}) - E(\text{BMP-TFSI}) \quad (4)$$

where E(adsorption complex) is the energy of the respective adsorption complex and E(Na) denotes the energy of the bare Na(0001) surface. E(BMP-TFSI) denotes the energy of an BMP-TFSI ion pair calculated within a large box (25 Å×26 Å×22 Å), employing only the Γ-point for the integration over the first Brillouin zone.

Electronic charges of atoms in molecules or adsorption complexes were evaluated according to the charge partitioning scheme proposed by Bader.[72–75]

Core level binding energies (BE) of atoms of various adsorption atoms or complexes were calculated according to Equation (5) as difference between the total energies of a final state, in which the core electron (X) is excited to the valence states (E^f(X)), and of the initial ground state (E^i),

$$BE^{calc}(X) = E^f(X) - E^i \quad (5)$$

employing the implementation in VASP developed by Köhler and Kresse.[76]

Calculated core level binding energies (BE^{calc}(X)) were then calibrated against experiment (see Equation (6)) using the experimental values of core level BEs of intact TFSI adsorbed on HOPG at a monolayer coverage of BMP-TFSI[30] as reference:

$$BE(X) = BE^{calc}(X) + BE^{exp}(X_{TFSI}) - BE^{calc}(X_{TFSI}) \quad (6)$$

where X or X_{TFSI} denote N 1s, C 1s, F 1s, O 1s or S 2p levels.

Calculations of BEs have been described in further detail in our previous publications.[32,33]

The convergence of the calculations has been checked by studies with increasing number of atomic layers of the surface slab and of the k-points as well as by comparison of two different PAW potentials for Na. The respective results are given in the Tables S1–S3 in the Supporting Information. These studies indicated only minor to negligible differences in the adsorption energy or N 1s core level binding energy for increasing accuracy of the parameters, and thus justified the choice of the parameters given above.

© 2023 The Authors. Batteries & Supercaps published by Wiley-VCH GmbH

25666223, 2023, 12, Downloaded from https://chemistry-europe.onlinelibrary.wiley.com/doi/10.1002/batt.202300336 by Cochrane Germany, Wiley Online Library on [06/12/2023]. See the Terms and Conditions (https://onlinelibrary.wiley.com/terms-and-conditions) on Wiley Online Library for rules of use; OA articles are governed by the applicable Creative Commons License

Acknowledgements

We gratefully acknowledge financial support from the German Research Foundation (DFG) under project ID 390874152 (POLiS Cluster of Excellence, EXC 2154) and project BE 1201/22-1, as well as computer time provided by the state of Baden-Württemberg through bwHPC and the DFG through grant no. INST 40/575-1 FUGG (JUSTUS 2 cluster). The work contributes to the research performed at CELEST (Center for Electrochemical Energy Storage Ulm-Karlsruhe). Open Access funding enabled and organized by Projekt DEAL.

Conflict of Interests

The authors declare no conflict of interest.

Data Availability Statement

The data that support the findings of this study are available from the corresponding author upon reasonable request.

Keywords: adsorption · solid electrolyte interphase · sodium · ionic liquids · photoelectron spectroscopy · density functional calculations

[1] A. Ponrouch, D. Monti, A. Boschin, B. Steen, P. Johansson, M. R. Palacin, *J. Mater. Chem. A* **2015**, *3*, 22.
[2] J. Y. Hwang, S. T. Myung, Y .K. Sun, *Chem. Soc. Rev.* **2017**, *46*, 3529.
[3] N. Tapia-Ruiz, A. R. Armstrong, H. Alptekin, M. A. Amores, H. Au, J. Barker, R. Boston, W. R. Brant, J. M. Brittain, Y. Chen, M. Chhowalla, Y. S. Choi, S. I. R. Costa, M. Crespo Ribadeneyra, S. A. Cussen, E. J. Cussen, W. I. F. David, A. V. Desai, S. A. M. Dickson, E. I. Eweka, J. D. Forero-Saboya, C. P. Grey, J. M. Griffin, P. Gross, X. Hua, J. T. S. Irvine, P. Johansson, M. O. Jones, M. Karlsmo, E. Kendrick, E. Kim, O. V. Kolosov, Z. Li, S. F. L. Mertens, R. Mogensen, L. Monconduit, R. E. Morris, A. J. Naylor, S. Nikman, C. A. O'Keefe, D. M. C. Ould, R. G. Palgrave, P. Poizot, A. Ponrouch, S. Renault, E. M. Reynolds, A. Rudola, R. Sayers, D. O. Scanlon, S. Sen, V. R. Seymour, B. Silván, M. T. Sougrati, L. Stievano, G. S. Stone, C. I. Thomas, M. M. Titirici, J. Tong, T. J. Wood, D. S. Wright, R. Younesi, *J. Phys. Energy* **2021**, *3*, 031503.
[4] I. Hasa, S. Mariyappan, D. Saurel, P. Adelhelm, A. Y. Koposov, C. Masquelier, L. Croguennec, M. Casas-Cabanas, *J. Power Sources* **2021**, *482*, 228872.
[5] I. Hasa, N. Tapia-Ruiz, M. Galceran, *Front. Energy Res.* **2022**, *10*, 10.3389/fenrg.2022.1076764.
[6] J. Zhao, J. Fu, J. Wang, K. Tang, Q. Liu, J. Huang, *J. Phys. Chem. C* **2022**, *126*, 15167.
[7] C. Vaalma, D. Buchholz, M. Weil, S. Passerini, *Nat. Rev. Mater.* **2018**, *3*, 18013.
[8] L. Wang, J. Song, R. Qiao, L. A. Wray, M. A. Hossain, Y. D. Chuang, W. Yang, Y. Lu, D. Evans, J. J. Lee, S. Vail, X. Zhao, M. Nishijima, S. Kakimoto, J. B. Goodenough, *J. Am. Chem. Soc.* **2015**, *137*, 2548.
[9] W. Zuo, A. Innocenti, M. Zarrabeitia, D. Bresser, Y. Yang, S. Passerini, *Acc. Chem. Res.* **2023**, *56*, 284.
[10] T. Welton, *Chem. Rev.* **1999**, *99*, 2071.
[11] M. Armand, F. Endres, D. R. MacF, H. Ohno, B. Scrosati, *Nat. Mater.* **2009**, *8*, 621.
[12] G. A. Giffin, *J. Mater. Chem. A* **2016**, *4*, 13378.
[13] T. Vogl, C. Vaalma, D. Buchholz, M. Secchiaroli, R. Marassi, S. Passerini, A. Balducci, *J. Mater. Chem. A* **2016**, *4*, 10472.
[14] H. Sun, G. Zhu, X. Xu, M. Liao, Y. Y. Li, M. Angell, M. Gu, Y. Zhu, W. H. Hung, J. Li, Y. Kuang, Y. Meng, M. C. Lin, H. Peng, H. Dai, *Nat. Commun.* **2019**, *10*, 3302.
[15] K. Sirengo, A. Babu, B. Brennan, S. C. Pillai, *J. Energy Chem.* **2023**, *81*, 321.
[16] J. Serra Moreno, G. Maresca, S. Panero, B. Scrosati, G. B. Appetecchi, *Electrochem. Commun.* **2014**, *43*, 1.
[17] A. Fukunaga, T. Nohira, R. Hagiwara, K. Numata, E. Itani, S. Sakai, K. Nitta, *J. Appl. Electrochem.* **2016**, *46*, 487.
[18] I. Hasa, S. Passerini, J. Hassoun, *J. Power Sources* **2016**, *303*, 203.
[19] L. G. Chagas, S. Jeong, I. Hasa, S. Passerini, *ACS Appl. Mater. Interfaces* **2019**, *11*, 22278.
[20] R. Hagiwara, K. Matsumoto, J. Hwang, T. Nohira, *Chem. Rec.* **2019**, *19*, 758.
[21] A. Massaro, J. Avila, K. Goloviznina, I. Rivalta, C. Gerbaldi, M. Pavone, M. F. Costa Gomes, A. A. H. Padua, *Phys. Chem. Chem. Phys.* **2020**, *22*, 20114.
[22] D. Monti, E. Jónsson, P. Palade, P. Johansson, *J. Power Sources* **2014**, *245*, 630.
[23] J. Song, B. Xiao, Y. Lin, K. Xu, X. Li, *Adv. Energy Mater.* **2018**, *8*, 1703082.
[24] L. Schafzahl, I. Hanzu, M. Wilkening, S. A. Freunberger, *ChemSusChem* **2017**, *10*, 401.
[25] G. G. Eshetu, M. Martinez-Ibanez, E. Sánchez-Diez, I. Gracia, C. Li, L. M. Rodriguez-Martinez, T. F. Rojo, H. Zhang, M. Armand, *Chem. Asian J.* **2018**, *13*, 2770.
[26] T. Hosokawa, K. Matsumoto, T. Nohira, R. Hagiwara, A. Fukunaga, S. Sakai, K. Nitta, *J. Phys. Chem. C* **2016**, *120*, 9628.
[27] M. Forsyth, M. Hilder, Y. Zhang, F. Chen, L. Carre, D. A. Rakov, M. Armand, D. R. MacFarlane, C. Pozo-Gonzalo, P. C. Howlett, *ACS Appl. Mater. Interfaces* **2019**, *11*, 43093.
[28] S. A. Ferdousi, L. A. O'Dell, M. Hilder, A. J. Barlow, M. Armand, M. Forsyth, P. C. Howlett, *ACS Appl. Mater. Interfaces* **2021**, *13*, 5706.
[29] F. Buchner, K. Forster-Tonigold, B. Uhl, D. Alwast, N. Wagner, A. Groß, R. J. Behm, *ACS Nano* **2013**, *7*, 7773.
[30] F. Buchner, K. Forster-Tonigold, M. Bozorgchenani, A. Gross, R. J. Behm, *J. Phys. Chem. Lett.* **2016**, *7*, 226.
[31] F. Buchner, B. Uhl, K. Forster-Tonigold, J. Bansmann, A. Groß, R. J. Behm, *J. Chem. Phys.* **2018**, *148*, 193821.
[32] F. Buchner, K. Forster-Tonigold, T. Bolter, A. Rampf, J. Klein, A. Groß, R. J. Behm, *J. Vac. Sci. Technol. A* **2022**, *40*, 023204.
[33] K. Forster-Tonigold, F. Buchner, J. Bansmann, R. J. Behm, A. Groß, *Batteries & Supercaps* **2022**, *5*, e202200307.
[34] J. F. Moulder, W. F. Stickle, P. E. Sobol, K. D. Bomben, *Handbook of X-ray Photoelectron Spectroscopy*, (Ed.: J. Chastain) Perkin Elmer Corp., Eden Prairie/USA **1992**.
[35] A. K. Shukla, R. S. Dhaka, C. Biswas, S. Banik, S. R. Barman, K. Horn, P. Ebert, K. Urban, *Phys. Rev. B* **2006**, *73*, 054432.
[36] M. Bender, K. Al-Shamery, H. J. Freund, *Langmuir* **1994**, *10*, 3081.
[37] A. Barrie, F. J. Street, *J. Electron Spectrosc. Relat. Phenom.* **1975**, *7*, 1.
[38] P. H. Citrin, *Phys. Rev. B* **1973**, *8*, 5545.
[39] A. Neumann, S. L. M. Schroeder, K. Christmann, *Phys. Rev. B* **1995**, *51*, 17007.
[40] P. Hofmann, D. Menzel, *Surf. Sci.* **1985**, *152 (153)*, 382.
[41] A. Böttcher, H. Niehus, *Phys. Rev. B* **1999**, *60*, 14396.
[42] J. Kim, F. Buchner, R. J. Behm, *J. Phys. Chem. C* **2020**, *124*, 21476.
[43] E. L. Garfunkel, X. Ding, G. Dong, S. Yang, X. Hou, X. Wang, *Surf. Sci.* **1985**, *164*, 511.
[44] F. Buchner, M. Bozorgchenani, B. Uhl, H. Farkhondeh, J. Bansmann, R. J. Behm, *J. Phys. Chem. C* **2015**, *119*, 16649.
[45] C. C. Hwang, K. S. An, R. J. Park, J. S. Kim, J. B. Lee, C. Y. Park, A. Kimura, A. Kakizaki, *J. Vac. Sci. Technol. A* **1998**, *16*, 1073.
[46] C. D. Wagner, *Faraday Discuss. Chem. Soc.* **1975**, *60*, 291.
[47] V. I. Nefedov, Y. Salyn, G. Leonhardt, R. Scheibe, *J. Electron Spectrosc. Relat. Phenom.* **1977**, *10*, 121.
[48] B. J. Lindberg, K. Hamrin, G. Johansson, U. Gelius, A. Fahlman, C. Nordling, K. Siegbahn, *Phys. Scripta* **1970**, *1*, 286.
[49] W. E. Swartz, K. J. Wynne, D. M. Hercules, *Anal. Chem.* **1971**, *43*, 1884.
[50] T. Yokoyama, A. Imanishi, S. Terada, H. Namba, Y. Kitajima, T. Ohta, *Surf. Sci.* **1995**, *334*, 88.
[51] C. D. Wagner, J. A. Taylor, *J. Electron Spectrosc. Relat. Phenom.* **1982**, *28*, 211.
[52] X. R. Yu, F. Liu, Z. Y. Wang, Y. Chen, *J. Electron Spectrosc. Relat. Phenom.* **1990**, *50*, 159.
[53] D. L. Doering, S. Semancik, *Surf. Sci.* **1983**, *129*, 177.
[54] B. V. Yakshinskiy, T. E. Madey, V. N. Ageev, *Surf. Rev. Lett.* **2000**, *07*, 75.
[55] J. K. Nørskov, T. Bligaard, A. Logadottir, S. Bahn, L. B. Hansen, M. Bollinger, H. Bengaard, B. Hammer, Z. Sljivancanin, M. Mavrikakis, Y. Xu, S. Dahl, C. J. H. Jacobsen, *J. Catal.* **2002**, *209*, 275.

© 2023 The Authors. Batteries & Supercaps published by Wiley-VCH GmbH

25666223, 2023, 12, Downloaded from https://chemistry-europe.onlinelibrary.wiley.com/doi/10.1002/batt.202300336 by Cochrane Germany, Wiley Online Library on [06/12/2023]. See the Terms and Conditions (https://onlinelibrary.wiley.com/terms-and-conditions) on Wiley Online Library for rules of use; OA articles are governed by the applicable Creative Commons License

[56] Y. Preibisch, F. Horsthemke, M. Winter, S. Nowak, A. S. Best, *Chem. Mater.* **2020**, *32*, 2389.
[57] R. Atkin, S. Z. E. Abedin, R. Hayes, L. H. S. Gasparotto, N. Borisenko, F. Endres, *J. Phys. Chem. C* **2009**, *113*, 13266.
[58] R. Atkin, N. Borisenko, M. Drüschler, S. Z. El Abedin, F. Endres, R. Hayes, B. Huber, B. Roling, *Phys. Chem. Chem. Phys.* **2011**, *13*, 6849.
[59] R. Wen, B. Rahn, O. M. Magnussen, *Angew. Chem. Int. Ed.* **2015**, *54*, 6062.
[60] R. Wen, B. Rahn, O. M. Magnussen, *J. Phys. Chem. C* **2016**, *120*, 15765.
[61] T. Diemant, T. Hager, H. E. Hoster, H. Rauscher, R. J. Behm, *Surf. Sci.* **2003**, *541*, 137.
[62] C. J. Powell, A. Jablonski, *NIST Electron Inelastic-Mean-Free-Path Database*, 1.1 ed. National Institute of Standards and Technology, Gaithersburg **2000**.
[63] S. Tanuma, C. J. Powell, D. R. Penn, *Surf. Interface Anal.* **1994**, *21*, 165.
[64] H. Euchner, A. Gross, *Phys. Rev. Mater.* **2022**, *6*, 040302.
[65] G. Kresse, J. Furthmüller, *Comp. Mat. Sci.* **1996**, *6*, 15.
[66] G. Kresse, J. Furthmüller, *Phys. Rev. B* **1996**, *54*, 11169.
[67] P. E. Blöchl, *Phys. Rev. B* **1994**, *50*, 17953.
[68] G. Kresse, D. Joubert, *Phys. Rev. B* **1999**, *59*, 1758.
[69] B. Hammer, L. B. Hansen, J. K. Nørskov, *Phys. Rev. B* **1999**, *59*, 7413.
[70] S. Grimme, J. Antony, S. Ehrlich, H. Krieg, *J. Chem. Phys.* **2010**, *132*, 154104–19.
[71] J. D. Chai, M. Head-Gordon, *Phys. Chem. Chem. Phys.* **2008**, *10*, 6615.
[72] G. Henkelman, A. Arnaldsson, H. Jonsson, *Comp. Mat. Sci.* **2006**, *36*, 354.
[73] E. Sanville, S. D. Kenny, R. Smith, G. Henkelman, *J. Comput. Chem.* **2007**, *28*, 899.
[74] W. Tang, E. Sanville, G. Henkelman, *J. Phys. Condens. Matter* **2009**, *21*, 084204.
[75] M. Yu, D. R. Trinkle, *J. Chem. Phys.* **2011**, *134*, 064111.
[76] L. Köhler, G. Kresse, *Phys. Rev. B* **2004**, *70*, 165405.

Manuscript received: July 27, 2023
Revised manuscript received: September 23, 2023
Accepted manuscript online: October 2, 2023
Version of record online: October 23, 2023

© 2023 The Authors. Batteries & Supercaps published by Wiley-VCH GmbH

25666223, 2023, 12, Downloaded from https://chemistry-europe.onlinelibrary.wiley.com/doi/10.1002/batt.202300336 by Cochrane Germany, Wiley Online Library on [06/12/2023]. See the Terms and Conditions (https://onlinelibrary.wiley.com/terms-and-conditions) on Wiley Online Library for rules of use; OA articles are governed by the applicable Creative Commons License